MAGNETIC FIELD DISTRIBUTION AND DESIGN OF HELMHOLTZ COILS

AR-006-355

JULIAN VRBANCICH

MRL-TR-91-8

MATERIALS RESEARCH LABORATORY

DSTO

Magnetic field distribution within uniform current density coils of non-zero cross-section and the design of Helmholtz coils

Julian Vrbancich

MRL-TR-91-8

CORRIGENDA

Please note the following corrections are required in this report.

p. 8 Equation 1 should be

$$H_z(z,0) = \frac{I}{2} \frac{a^2}{(a^2 + z^2)^{3.2}} \qquad (1)$$

p. 36 Figure 18: $Pa_1 = 0.3$ should be $P/a_1 = 0.3$.

p. 38 Paragraph 1, line 3: $\propto = 1.01$ should be $\propto = 1.02$.

p. 56 Paragraph 4, line 4: designed should be designated.

Magnetic Field Distribution Within Uniform Current Density Coils of Non-zero Cross-section and the Design of Helmholtz Coils

Julian Vrbancich

MRL Technical Report
MRL-TR-91-8

Abstract

A uniform magnetic field is required to calibrate magnetic induction sensor coils. Two types of coil designs are considered; a single finite length solenoid and a coaxially split coil pair (Helmholtz coil). The design must be able to reliably predict the magnitude of the calibration field and its homogeneity, both radially and axially, to within certain tolerances. The experimental results of a design based on the split coil pair are given. Furthermore, it is suggested that the quasi-uniform field in the mid-plane of a split coil pair can be usefully extended by narrowing the gap of the conventional Helmholtz coil pair spacing. In such cases, the flux in a circular region in the mid-plane can approach the value that would exist for a perfectly uniform field because of the partial cancellation between fields greater than and less than the central field. The deviation of the central field from that of an infinitely long solenoid is also discussed.

MATERIALS RESEARCH LABORATORY

Published by

DSTO Materials Research Laboratory
Cordite Avenue, Maribyrnong
Victoria, 3032 Australia

Telephone: (03) 319 3887
Fax: (03) 318 4536

AR No. 006-355

APPROVED FOR PUBLIC RELEASE

Author

Julian Vrbancich

Julian Vrbancich obtained his PhD in Chemical Physics at the University of Sydney in 1979 and has held post-doctoral appointments at the University of Bologna, Italy, University of Glasgow, UK and the ANU, Australia. In 1984 he joined the Royal Australian Navy Research Laboratory, Sydney (later transferred to MRL in 1987) and began research and development in the area of underwater propagation and detection of ELF electromagnetic fields. His research interests include electric and magnetic field sensors design, signal processing and numerical modelling and experimental verification of subsurface electromagnetic propagation.

Contents

Magnetic Field Distribution Within Uniform Current Density Coils of Non-Zero Cross-Section and the Design of Helmholtz Coils

1. Introduction

It is often necessary to have a source for a uniform magnetic field, for example, to provide a field of known uniformity and magnitude for calibration purposes. A single coil is easier to construct than a combination of two or more coils but its field homogeneity may be inadequate; thus a quantitative comparison is required. Furthermore, there appears to be a paucity of data and tables available in the literature that allow the design of a system to generate a homogeneous field over a given region. The coil geometries represented in the available tables can be too restrictive and the given error limits or uniformity tolerances may be unsuitable. Another important feature which is not emphasized is the field uniformity of a slightly uncompensated coil pair having a gap which differs from the optimum coil pair spacing of a true Helmholtz coil. Such a coil can generate a nearly uniform field over a larger region than the true Helmholtz coil. If the flux of the axial field is required, then the introduced error is improved significantly because of the possible cancellation of field non-uniformities.

In this report, a brief description of solenoid design is given in terms of the geometry of the coil [1]. There are two reasons for examining these details. Firstly, it enables the axial field homogeneity to be determined at radial distances away from the coil centre. Secondly, as pairs of coils will be considered as candidates for providing homogeneous fields, the formalism introduced here for the single coil will also apply to more complex coil designs.

1.1 *Magnetic Field at Centre of a Coil of Non-zero Cross-section*

The magnetic field along the axis of a circular current loop is (Fig. 1)

$$H_z(z,0) = \frac{I}{2}\frac{a^2}{2(a^2+z^2)^{3/2}} \tag{1}$$

where H is in units of $A\ m^{-1}$, a is the loop radius in m, z is the distance along the axis in m and I is the current (amps) in the conductor. Thus

$$\begin{aligned} H_0 &= H_z(0,0) \\ &= \frac{I}{2a} \end{aligned} \tag{2}$$

and

$$H_z(z,0) = H_0\frac{a^3}{(a^2+z^2)^{3/2}}. \tag{3}$$

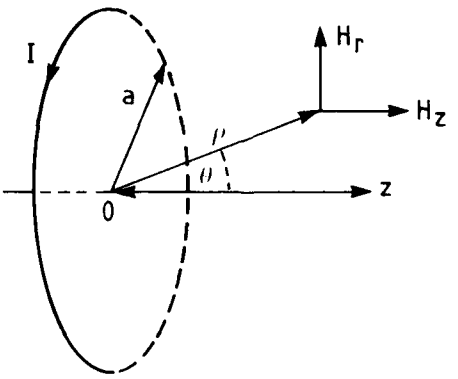

Figure 1: Magnetic field components for a circular current loop; H_r and H_z are the radial and axial components respectively.

The coil geometry is defined in terms of two parameters α and β, see Figure 2. In this report, where appropriate in mathematical expressions, the following symbols will be used for dimensionless distances: $\xi = r/a_1$ ($\theta = \pi/2$), $\gamma = z/a_1$ ($\theta = 0$) and ρ/a_1 ($\theta \neq \pi/2$, $\theta \neq 0$). Either expression (e.g. ξ or r/a_1) will be used interchangably.

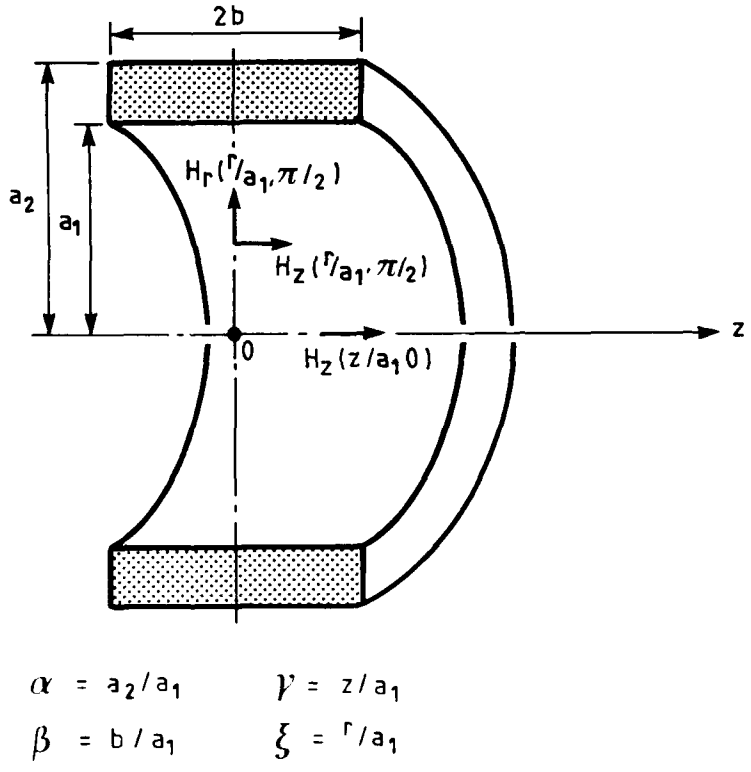

Figure 2: Definition of coil geometry parameters α and β for a coil of non-zero cross-section. For a current sheet $a_1 \rightarrow a_2 = a$, and $\cos\theta = b/(a^2 + b^2)^{1/2}$, $\alpha = 1$, $\beta = b/a$.

The current density is j (Am^{-2}) (= I_{total}/cross-section area) and for N turns of uniform current density,

$$j = \frac{NI}{2b(a_2 - a_1)}. \qquad (4)$$

If the space factor λ (which represents the active cross-sectional area of the windirg divided by the total cross-sectional area) is not unity, then

$$j = j_c \lambda \tag{5}$$

where j_c is the current density in the conductor. As $a_1 \rightarrow a_2$, a current sheet obtains, i.e. $I' = NI/2b$, however, now I' is equivalent to current per unit length and $I \propto \int_{-b}^{+b} I'\, dz$. Thus H_0 for a current sheet obtains from eqn. 1

$$\begin{aligned} H_0 &= \frac{1}{2} \int_{-b}^{+b} \frac{I' a^2}{(a^2 + z^2)^{3/2}}\, dz \\ &= \frac{NI}{2\sqrt{a^2 + b^2}} \end{aligned} \tag{6}$$

1.1.1 Non-zero Cross-section Coil

For a non-zero cross-section coil (Fig. 2), the field at the centre of the coil H_0 is given by (see eqn. 1)

$$\begin{aligned} H_0 &= \frac{j_c \lambda}{2} \int_{a_1}^{a_2} \int_{-b}^{+b} \frac{r^2}{(r^2 + z^2)^{3/2}}\, dz\, dr \\ &= j_c \lambda a_1 \beta \ln\left(\frac{\alpha + (\alpha^2 + \beta^2)^{1/2}}{1 + (1 + \beta^2)^{1/2}} \right). \end{aligned} \tag{7}$$

The field H_0 is significant in the following analysis because the fields at any point along the axis, or away from the axis may be expressed in terms of the central field H_0. Furthermore, this also applies to the case of *multiple* concentric coils.

One may conveniently separate an entirely geometry-dependent field factor $F(\alpha, \beta)$ from eqn. 7 so that H_0 can be readily estimated from values of $F(\alpha, \beta)$ represented in graphical form (see Figs 3 and 4) or tabular form, and the variation in H_0 as a function of coil geometry can also be readily determined.

$$F(\alpha,\beta) = \beta \times \ln\left(\frac{\alpha + (\alpha^2 + \beta^2)^{1/2}}{1 + (1 + \beta^2)^{1/2}} \right) \tag{8}$$

$$= \beta\left[\sinh^{-1}(\alpha/\beta) - \sinh^{-1}(1/\beta) \right]. \tag{9}$$

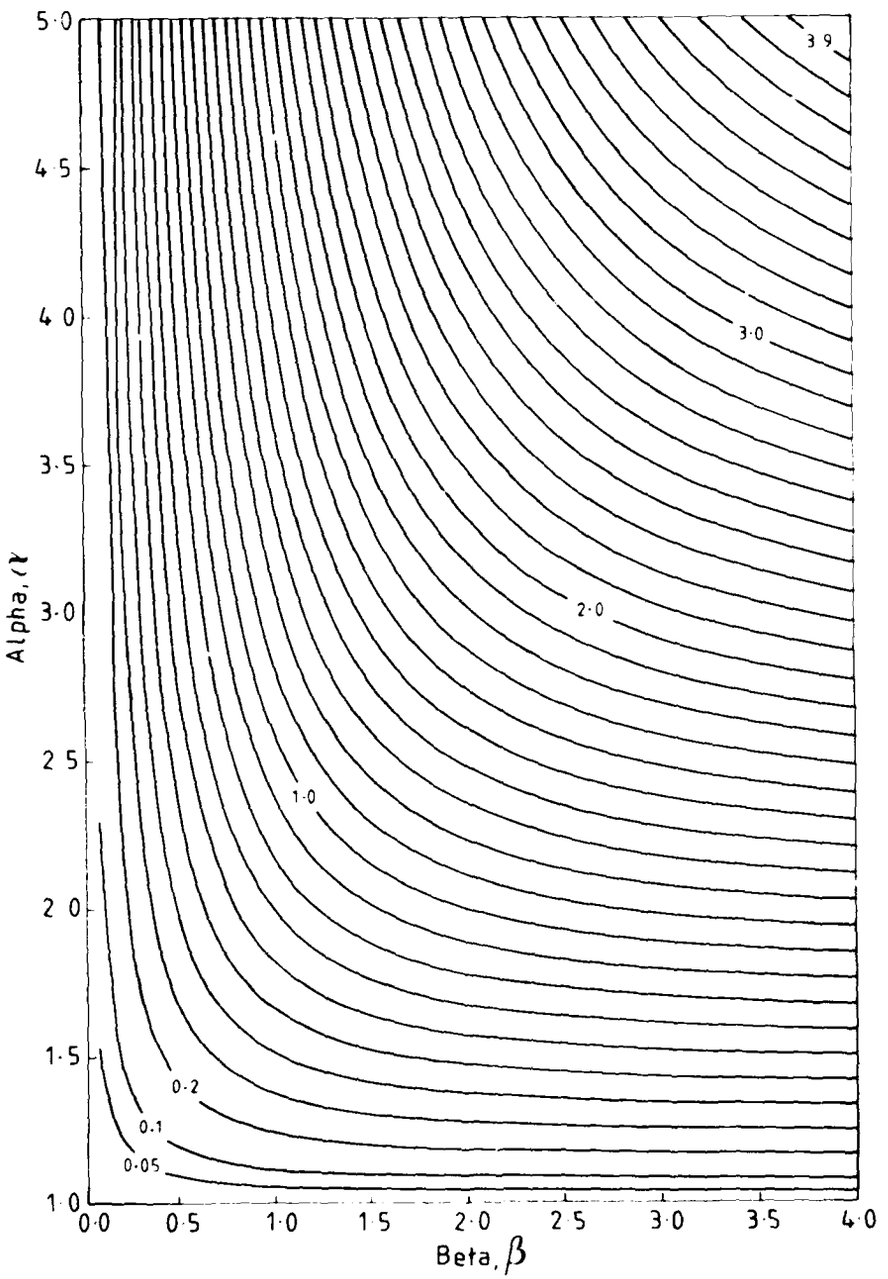

Figure 3: *Geometry dependent field factors* $[(4\pi/10)F(\alpha, \beta) = 0.05, 0.1\ (0.1)\ 3.9$ *in terms of* α *and* β *coil geometry parameters.*

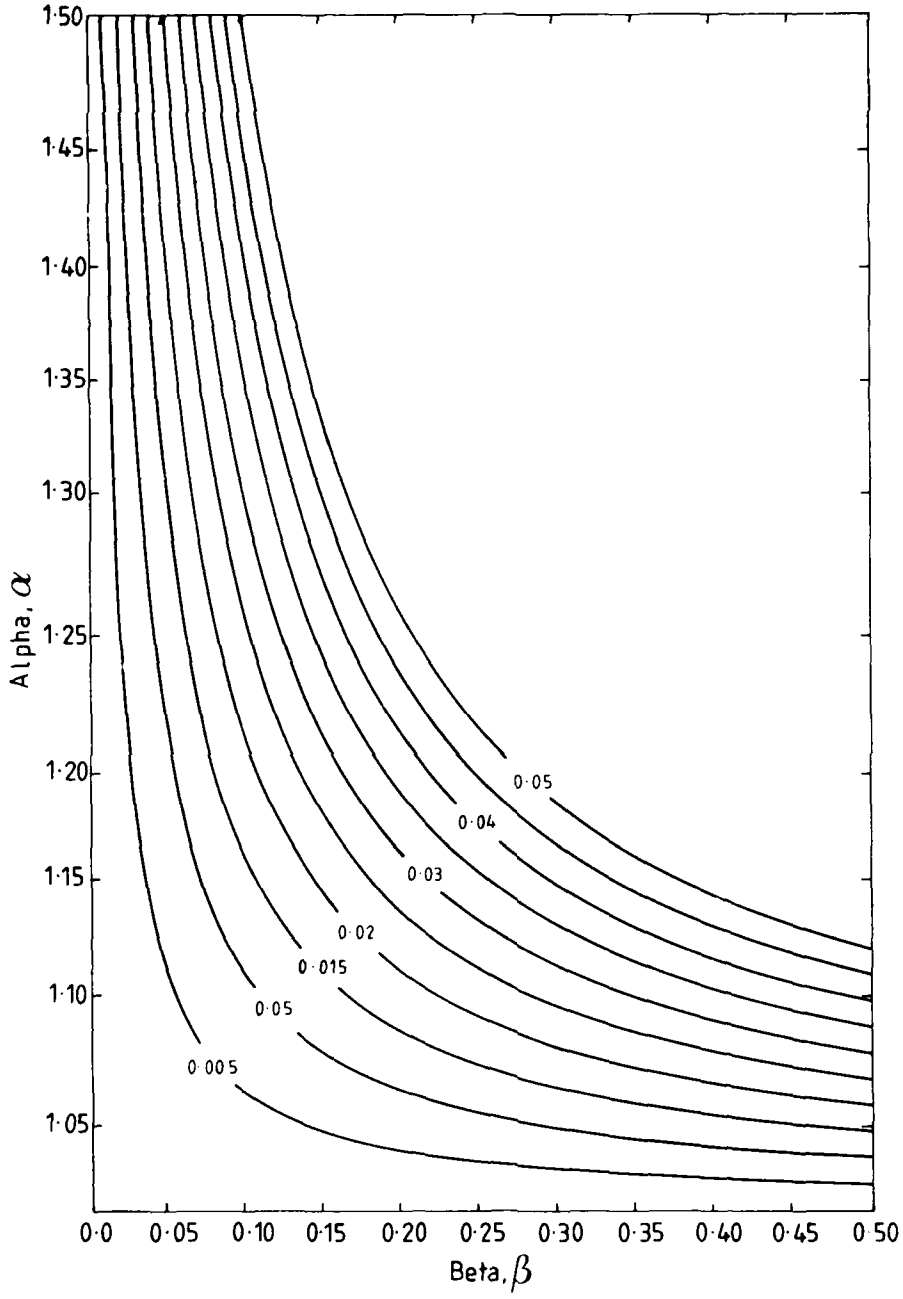

Figure 4: Geometry dependent field factors [(4π/10)F(α, β) = 0.005 (0.005) 0.05 in terms of α and β.

Note that

$$F(\alpha, -\beta) = -F(\alpha,\beta). \tag{10}$$

Now

$$H_0 = j_c \lambda a_1 F(\alpha,\beta) = \left(\frac{NI}{2\beta a_1(\alpha-1)}\right) F(\alpha,\beta). \tag{11}$$

1.1.2 *Deviation of a Field from an Infinitely Long Solenoid*

Figures 3 and 4 also display the variation in H_0 from the ideal infinitely long solenoid given by $H = nI$ where $n(= N/2\beta a_1)$ is the turns per unit length. For example, for a fixed small value of $\alpha(\alpha = 1.5)$, $F(\alpha, \beta)$ is approximately constant for β greater than 2.0 and thus H_0 is proportional to nI for a coil having a dimensionless length of $2\beta > 4.0$. Taking this point further, as $\beta \rightarrow \infty$, eqn. 9 gives

$$F(\alpha,\beta) = (\alpha - 1) - \frac{(\alpha^3 - 1)}{6\beta^2} + \frac{3(\alpha^5 - 1)}{40\beta^4} - \ldots \tag{12}$$

It is clear that the central field of a real solenoid, Eqn. 11, approaches that of an infinitely long solenoid, when $F(\alpha, \beta)/(\alpha - 1) \rightarrow 1.0$. In Figure 5, the deviation factor $F(\alpha, \beta)/(\alpha - 1)$ is plotted as a function of the normalized coil length (2β) for various normalized coil thicknesses $(\alpha - 1)$. It is now easy to visualize to what extent the coil thickness and length affects the deviation of the central field from that of an infinitely long solenoid $(F(\alpha, \beta)/(\alpha - 1) = 1.0)$.

2. *Non-Central Field*

2.1 *Introduction*

The axial field away from the centre of the coil, $H_z(r/a_1, \pi/2)$, see Figure 2, may be computed from published tables given by Hart [2]. Whilst these are comprehensive, there are several disadvantages. Interpolation may be required (over a surface or line) and the tables do not easily lend themselves to the calculation of parameters required to attain a specific field homogeneity, either from one coil or by a combination of several coils. One useful feature of Hart's tables is that the fields may be computed at points well away from the central

region of the coil, even at points within the current distribution, provided the current flow is uniform.

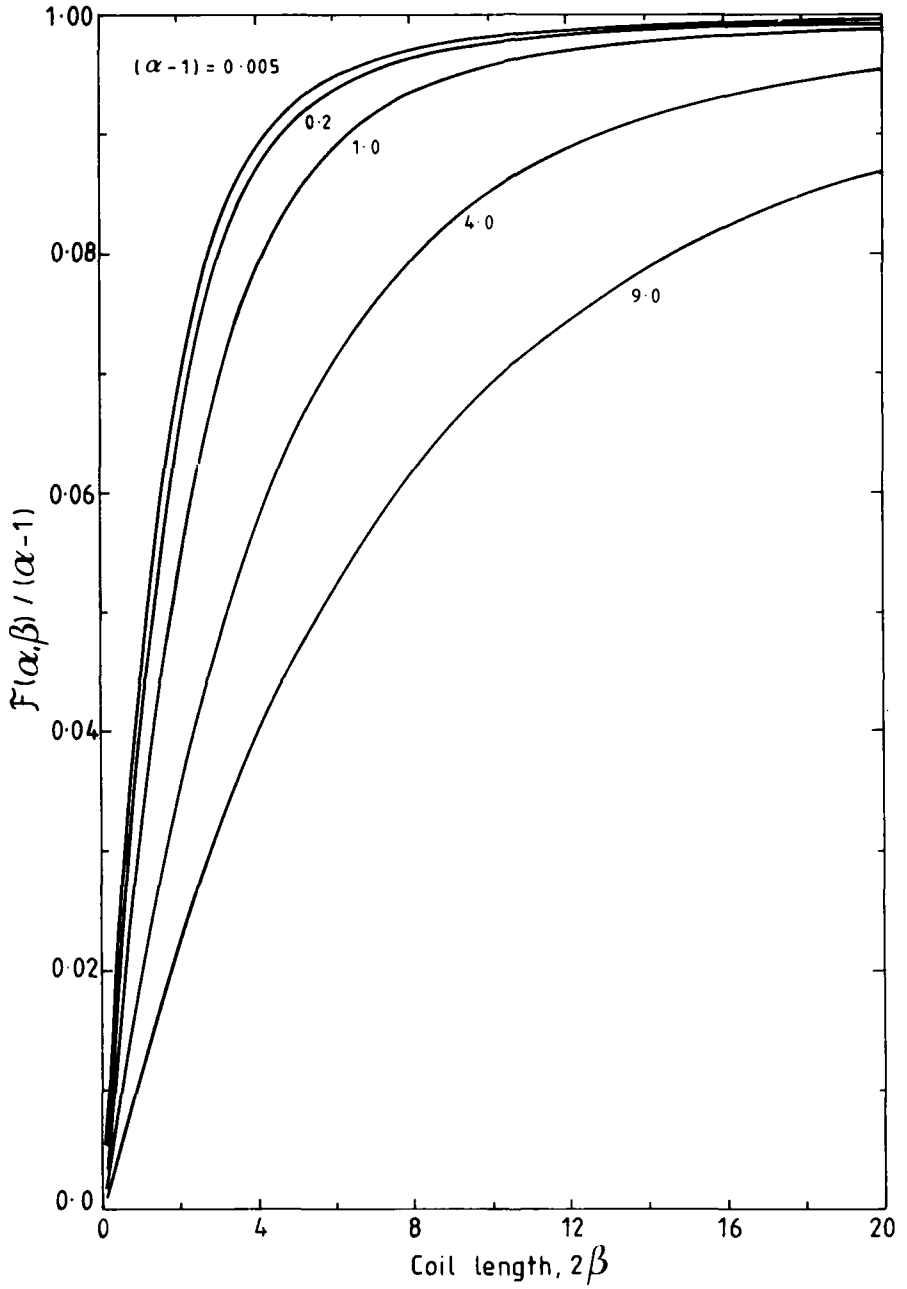

Figure 5: The deviation factor F(α, β)/(α - 1) as a function of coil length 2β for various coil thicknesses (α - 1).

A superior technique introduced by Garrett [3] treats the field of an axially symmetric system as an expansion of zonal harmonics (legendre polynomials). The significance of this approach is that the field at any point in the *vicinity* of the origin can be expressed as an infinite series of terms involving simple algebraic expressions. The vicinity specifies a central region whose boundary is a sphere that contains no field source and satisfies Laplace's equation. (A source is any discontinuity of the windings, for example, the boundary edge of a solenoid.) Thus the distinctive feature of the zonal harmonic method is that it permits a clean separation of the field geometry from that of the generating system and it allows the field to be described as a continuous scalar function of the field coordinates [4].

2.2 *Field in a Central Zone*

The magnetic field in the central zone of a cylindrically symmetric magnet can be written as a power series, involving Legendre polynomials, which converges everywhere within a sphere excluding any field source. If the origin is on the midplane of symmetry, the series expansion will have only even terms and the axial and radial fields, H_z and H_r, can be expressed as [3], [5]

$$H_z(\rho,\theta) = \sum_{n=1}^{\infty} \frac{1}{(2n-2)!} H_z^{(2n-2)}(0,0)\rho^{2n-2} P_{2n-2}(u) \tag{13}$$

$$H_r(\rho,\theta) = -\sin\theta \sum_{n=1}^{\infty} \frac{1}{(2n-1)!} H_z^{(2n-2)}(0,0)\,\rho^{2n-2} P'_{2n-2}(u) \tag{14}$$

where

$$H_z^{(2n-2)}(0,0) = \left(\frac{d^{2n-2} H_z(z,0)}{dz^{2n-2}}\right)_{z=0}, \tag{15}$$

$P_n(u)$ and $P'_n(u)$ are respectively the Legendre polynomials and their first derivatives with respect to cos θ (u = cos θ), see Table 1, and ρ and θ are defined in Figure 1. Equations 13 and 14 reduce to [1], [5]

$$H_z(\rho/a_1,\theta) = H_0[1 + E_2(\rho/a_1)^2 P_2(u) + E_4(\rho/a_1)^4 P_4(u) + \ldots] \tag{16}$$

$$H_r(\rho/a_1,\theta) = H_0[0 - \frac{E_2}{3}(\rho/a_1)^2 P'_2(u) - \frac{E_4}{5}(\rho/a_1)^4 P'_4(u) - \ldots]\sin\theta \tag{17}$$

where H_0 is defined in eqn. 7,

$$E_{2n} = \frac{1}{H_0(2n)!}\left(\frac{d^{2n}H_z(z,0)}{dz^{2n}}\right)_{z=0} \tag{18}$$

and E_{2n}, for a uniform current density coil [1], are given in Table 2. Note that in eqns. 16 and 17, the fields in a region of space around the origin depend only on H_0 and a geometry factor.

Table 1: Even order Legendre polynomials and their first derivative with respect to cos θ, $u = \cos\theta$

$P_0(u) = 1$	$P'_0(u) = 0$
$P_2(u) = 1/2\ (3u^2 - 1)$	$P'_2(u) = (6u)/2$
$P_4(u) = 1/8\ (35u^4 - 30u^2 + 3)$	$P'_4(u) = 1/8\ (140u^3 - 60u)$
$P_6(u) = 1/16\ (231u^6 - 315u^4 + 105u^2 - 5)$	$P'_6(u) = 1/16\ (1386u^5 - 1260u^3 + 210u)$
$P_8(u) = 1/128\ (6435u^8 - 12012u^6 + 6930u^4 - 1260u^2 + 35)$	$P'_8(u) = 1/128\ (51480u^7 - 72072u^5 + 27720u^3 - 2520u)$
$u = 1\ (\theta = 0)$	$u = 0\ (\theta = \pi/2)$
$P_n(\pm 1) = (\pm 1)^n$	$P_n(0) = 0$ n : *odd*
$P'_n(\pm 1) = (\pm 1)^{n+1} \times n(n+1)/2$	$P_n(0) = (-1)^{n/2} \times [1.3.5..(n-1)/2.4.6..n]$ n : *even*
	$P'_n(0) = nP_{n-1}(0)$

As shown in section 3.1, the axial field at any point along the axis is

$$H_z(\gamma,0) = \frac{j_c\lambda a_1}{2}\left((\gamma+\beta)\ln\left[\frac{\alpha+[\alpha^2+(\gamma+\beta)^2]^{1/2}}{1+[1+(\gamma+\beta)^2]^{1/2}}\right] - (\gamma-\beta)\ln\left[\frac{\alpha+[\alpha^2+(\gamma-\beta)^2]^{1/2}}{1+[1+(\gamma-\beta)^2]^{1/2}}\right]\right) \tag{19}$$

where $\gamma = z/a_1$ is the distance along the z-axis normalized to the inside radius of the coil, see Figure 2. Equation 7 obtains when $\gamma = 0$.

Table 2: Error coefficients for uniform current density coils

$$C_1 = \frac{1}{1+\beta^2} \quad C_2 = \frac{\beta^2}{1+\beta^2} \quad C_3 = \frac{\alpha^2}{\alpha^2+\beta^2} \quad C_4 = \frac{\beta^2}{\alpha^2+\beta^2}$$

$$F(\alpha,\beta)E_2(\alpha,\beta) = \frac{1}{2\beta}[C_1^{3/2} - C_3^{3/2}]$$

$$F(\alpha,\beta)E_4(\alpha,\beta) = \frac{1}{24\beta^3}[C_1^{3/2}(2+3C_2+15C_2^2) - C_3^{3/2}(2+3C_4+15C_4^2)]$$

$$F(\alpha,\beta)E_6(\alpha,\beta) = \frac{1}{240\beta^5}[C_1^{3/2}(8+12C_2+15C_2^2-70C_2^3+315C_2^4) - C_3^{3/2}(8+12C_4+15C_4^2-70C_4^3+315C_4^4)]$$

$$F(\alpha,\beta)E_8(\alpha,\beta) = \frac{1}{896\beta^7}[C_1^{3/2}(16+24C_2+30C_2^2+35C_2^3+315C_2^4 - 2079C_2^5+3003C_2^6) - C_3^{3/2}(16+24C_4+30C_4^2+35C_4^3+315C_4^4 - 2079C_4^5+3003C_4^6)]$$

$$(dH_z/dz)_{z=0} = (d^3H_z/dz^3)_{z=0} = (d^{2n+1}H_z/dz^{2n+1})_{z=0} = 0$$

2.3 *Field Uniformity for a Single Coil*

Along the z-axis ($u = 1$, see Table 1), $H_r = 0$ by symmetry and H_z is given by eqn. 16,

$$H_z(\gamma,0) = H_0(1 + E_2(\alpha,\beta)\gamma^2 + E_4(\alpha,\beta)\gamma^4 + \ldots). \qquad (20)$$

Further, at $\theta = \pi/2$, the axial field is

$$H_z(\xi,\pi/2) = H_0[1 - \frac{1}{2}E_2(\alpha,\beta)\xi^2 + \frac{3}{8}E_4(\alpha,\beta)\xi^4 - \frac{5}{16}E_6(\alpha,\beta)\xi^6 + \frac{35}{128}E_8(\alpha,\beta)\xi^8 + \ldots]. \quad (21)$$

For a simple solenoid, $E_2(\alpha, \beta)$ is negative and the axial field decreases along the z-axis, eqn. 20. However, the axial field increases radially from the centre, eqn. 21. Close to the centre, where the $E_2(\alpha, \beta)$ term predominates, the axial field deviation from H_0 in the radial direction, $H_z(\xi, \pi/2)/H_0$, is only half that of the axial direction. Thus eqn. 20 can be used to determine a bound for the homogeneity of the axial field within a sphere of radius γ ($< a$) since the inhomogeneity associated with any individual term is greatest in the z direction (see also section 3.5).

It is now necessary to consider the uniformity of the axial field, in terms of coil geometry α and β, over a sphere of given radius as a percentage deviation of the central field, that is

$$\frac{H_z(\rho/a_1,\theta)}{H_0} = 1 + H' \quad (22)$$

where H' is obtained from eqns. 20 and 21 for $\theta = 0$ ($\rho/a_1 = \gamma$) and $\theta = \pi/2$ ($\rho/a_1 = \xi$) respectively. The ratio $H_z(\rho/a_1, \theta)/H_0$ has been evaluated for three values of ρ/a_1; 0.30, 0.50 and 0.707 ($1/\sqrt{2}$). The results are shown graphically in Figures 6 to 8. The terms in eqns. 20 and 21 were computed in double precision up to and including the eighth order contribution. This allowed the convergence of the series expansion to be examined. A selected number of $E_n(\alpha, \beta)\xi^n$ ($n = 2, 4, 6, 8$) results are given in Table 3; these are applicable to both $H_z(\gamma, 0)/H_0$ and $H_z(\xi, \pi/2)/H_0$. It is worth noting that the convergence of the $H_z(\xi, \pi/2)/H_0$ series is better than that indicated by Table 3 because the coefficients 1/2, 3/8, 5/16 and 35/128 were omitted to allow the results to apply to both series.

The convergence of the series expansion (eqns. 20 and 21) is such that for most values of α and β, only the first two terms are required, depending on the desired accuracy although clearly, more terms must be included as (ρ/a_1) approaches unity. However convergence is slow when β is small, especially when $\xi > 0.5$. As a worst case, when $\alpha = 1.01$ and $\beta = 0.1$, the eighth-order term $E_8(\alpha, \beta)\xi^8$ contributes respectively 0.1% [0.05%], 3% [0.9%] and 21% [5.4%] for (ρ/a_1) = 0.3, 0.5 and 0.707 in the series expansion of $H_z(\gamma, 0)/H_0$ and $H_z(\xi, \pi/2)/H_0$.

As shown in Figures 6 to 8, for a given coil thickness α, the deviation of the axial field from the central field decreases as the coil lengthens. Conversely, as the coil thickness increases for a fixed β, the deviation H_z/H_0 decreases. Furthermore, above $\beta \approx 1.5$ there is little change in H_z as a function of α and hence β appears to play the dominant role in determining field homogeneity. (This case approaches that of an infinitely long single layer solenoid, see section 1.1.2.) For lower values of β, the field homogeneity is sensitive to α. At

$\beta = 1.0$, $\xi = 0.707$, $H_z(\xi, \pi/2)/H_0$ varies by only 4% from 1.088 at $\alpha = 1.01$ to 1.053 at $\alpha = 5.0$. For $\xi = 0.5$, the variation is less than 2%.

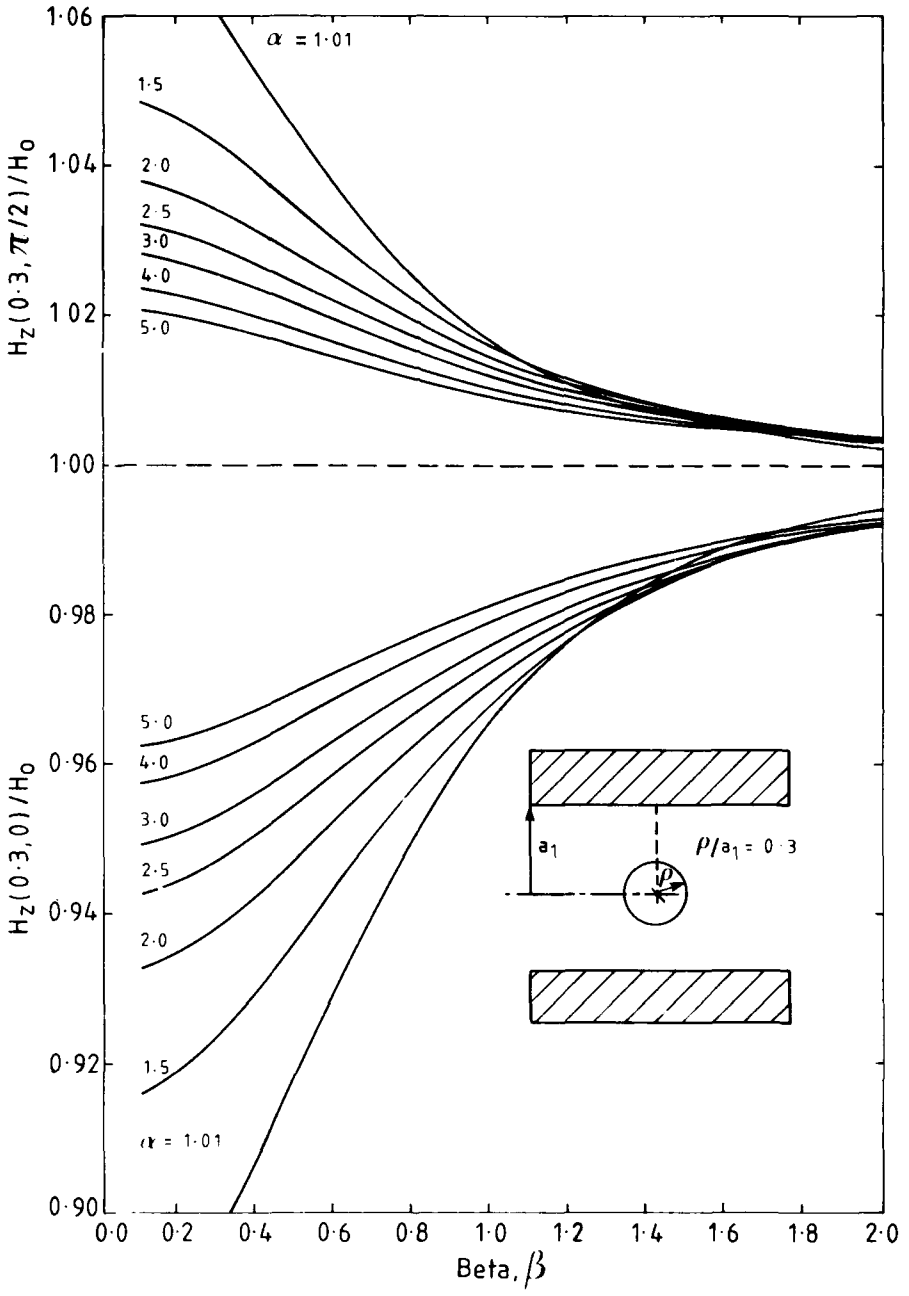

Figure 6: Deviation of axial fields $H_z(r/a_1, \pi/2)$ and $H_z(z/a_1, 0)$ from the central field H_0 of a single coil as a function of α and β for $\rho/a_1 = 0.3$.

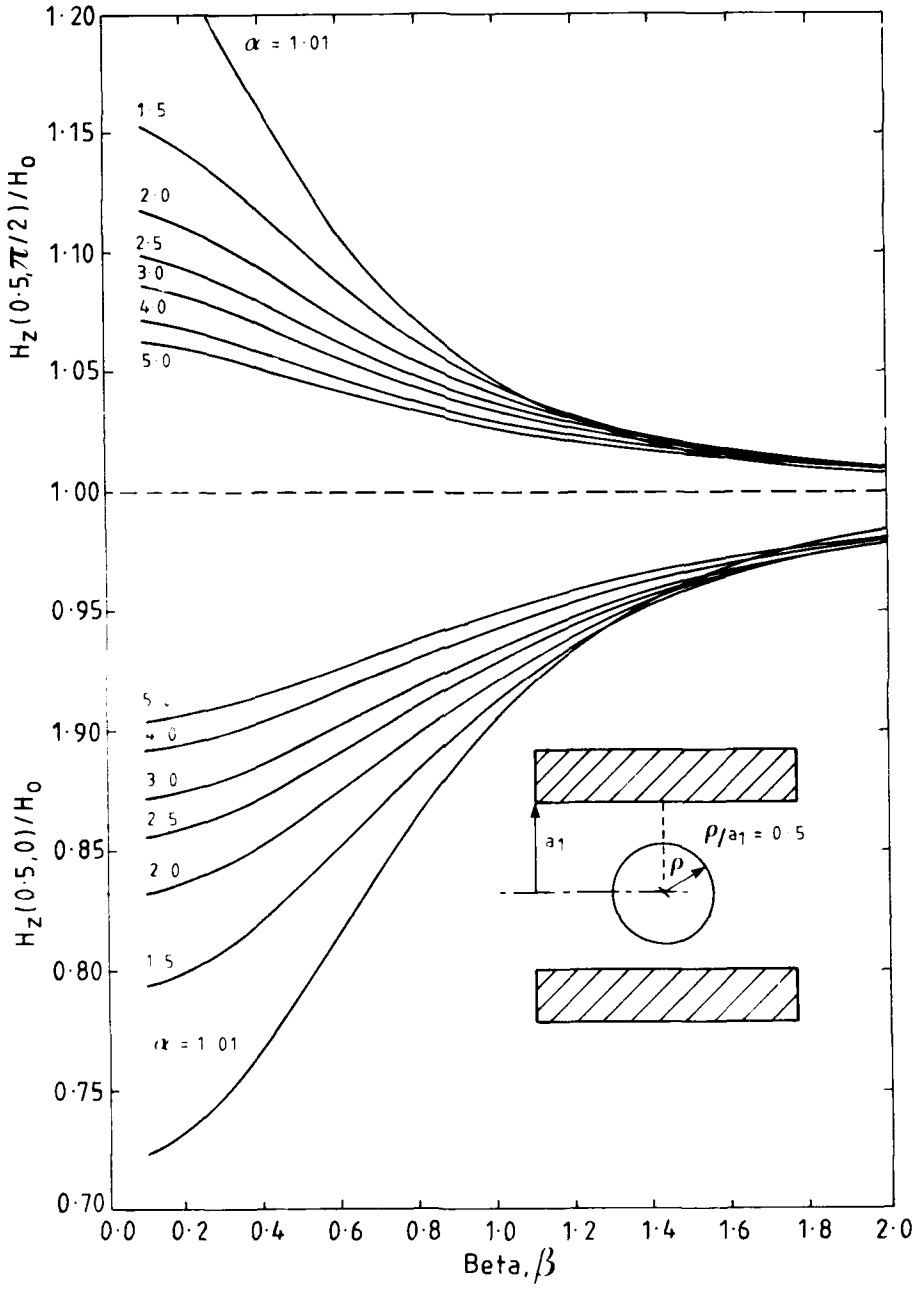

Figure 7: Deviation of axial fields $H_z(r/a_1, \pi/2)$ and $H_z(z/a_1, 0)$ from the central field H_0 of a single coil as a function of α and β for $\rho/a_1 = 0.5$.

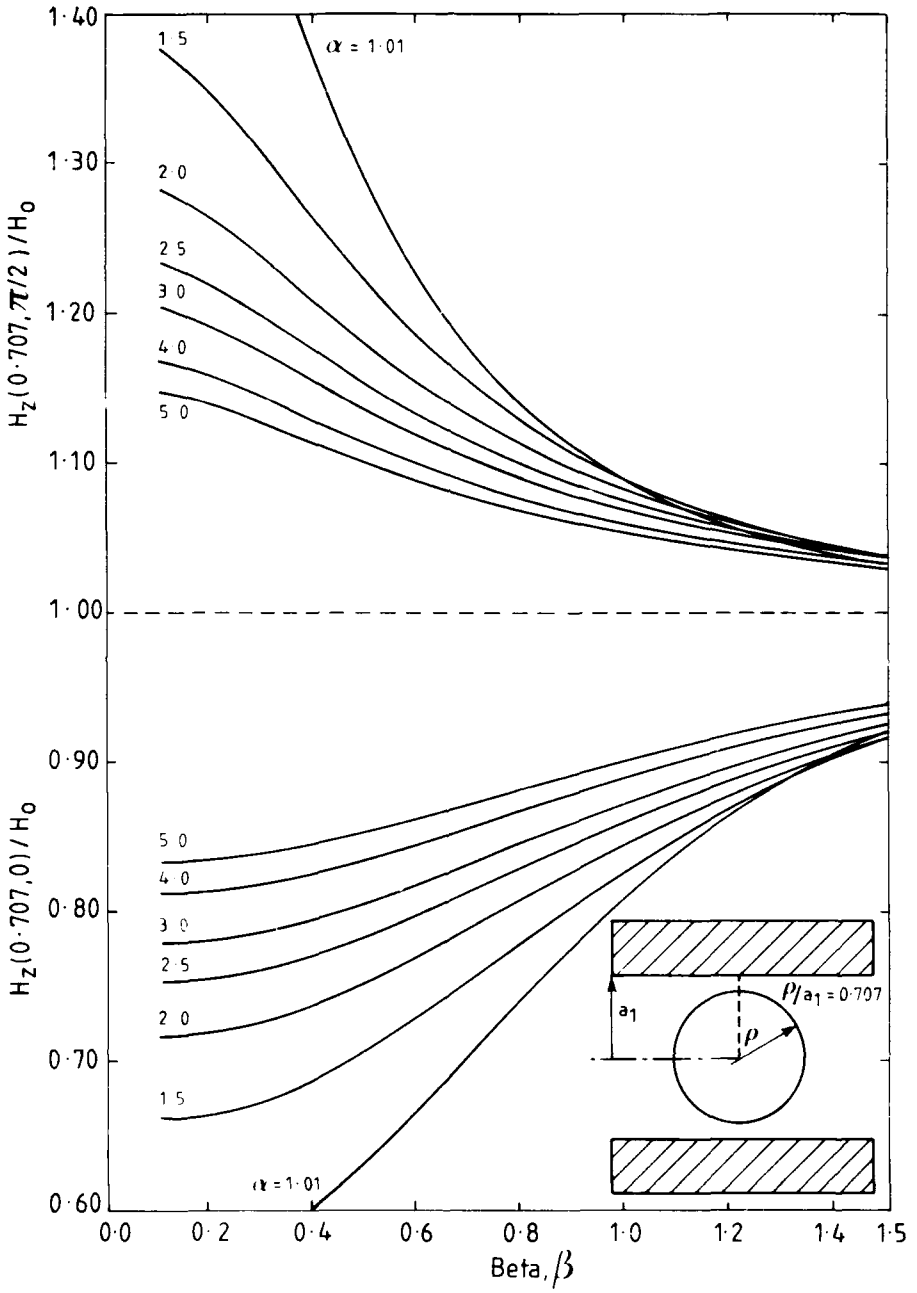

Figure 8: Deviation of axial fields $H_z(r/a_1, \pi/2)$ and $H_z(z/a_1, 0)$ from the central field H_0 of a single coil as a function of α and β for $\rho/a_1 = 0.707$.

Table 3: Selected values of $E_n(\alpha, \beta)\xi^n$ terms

α	β	$E_2(\alpha, \beta)\xi^2$	$E_4(\alpha, \beta)\xi^4$	$E_6(\alpha, \beta)\xi^6$	$E_8(\alpha, \beta)\xi^8$
			$\xi = 0.30$		
1.01	0.1	-1.31E-1	1.4E-2	-1.4E-3	1.3E-4
	1.0	-3.4 E-2	-3.0E-4	3.5E-5	4.5E-7
	2.0	-5.4 E-3	-1.1E-4	-1.1E-6	2.7E-9
	3.5	-7.8 E-4	-7.6E-6	-5.7E-8	-3.4E-10
	5.0	-2.0 E-4	-1.1E-6	-4.7E-9	-1.8E-11
2.0	0.1	-7.2 E-2	4.9E-3	-3.5E-4	2.5E-5
	1.0	-2.9 E-2	1.6E-4	1.2E-5	-1.7E-7
	2.0	-7.4 E-3	-6.9E-5	7.4E-8	9.2E-9
	3.5	-1.4 E-3	-1.0E-5	-4.8E-8	-1.2E-10
	5.0	-4.1 E-4	-1.9E-6	-6.4E-9	-1.7E-11
5.0	0.1	-4.0 E-2	2.3E-3	-1.5E-4	1.1E-5
	1.0	-1.9 E-2	1.3E-4	4.6E-6	-6.8E-8
	2.0	-6.9 E-3	-1.6E-5	1.2E-7	2.8E-9
	3.5	-2.2 E-3	-5.6E-6	-7.3E-9	4.1E-12
	5.0	-9.1 E-4	-1.9E-6	-2.4E-9	-1.9E-12
			$\xi = 0.50$		
1.01	0.1	-3.6 E-1	1.1E-1	-3.0E-2	7.9E-3
	1.0	-9.4 E-2	-2.3E-3	7.4E-4	2.7E-5
	2.0	-1.5 E-2	-8.1E-4	-2.3E-5	1.6E-7
	3.5	-2.2 E-3	-5.7E-5	-1.2E-6	-2.0E-8
	5.0	-5.6 E-4	-8.4E-6	-1.0E-7	-1.1E-9
2.0	0.1	-2.0 E-1	3.8E-2	-7.5E-3	1.5E-3
	1.0	-8.0 E-2	1.3E-3	2.7E-4	-1.0E-5
	2.0	-2.1 E-2	-5.3E-4	1.5E-6	5.4E-7
	3.5	-3.9 E-3	-7.9E-5	-1.0E-6	-7.1E-9
	5.0	-1.1 E-3	-1.4E-5	-1.4E-7	-1.0E-9
5.0	0.1	-1.1 E-1	1.75E-2	-3.3E-3	6.5E-4
	1.0	-5.1 E-2	1.0 E-3	9.8E-5	-4.0E-6
	2.0	-1.9 E-2	-1.3 E-4	2.5E-6	1.7E-7
	3.5	-6.2 E-3	-4.3 E-5	-1.6E-7	2.5E-10
	5.0	-2.5 E-3	-1.5 E-5	-5.1E-8	-1.1E-10
			$\xi = 0.707$		
1.01	0.1	-7.3E-1	4.4E-1	-2.4E-1	1.3E-1
	1.0	-1.9E-1	-9.4E-3	5.9E-3	4.3E-4
	2.0	-3.0E-2	-3.2E-3	-1.8E-4	2.5E-6
	3.5	-4.3E-3	-2.3E-4	-9.7E-6	-3.2E-7
	5.0	-1.1E-3	-3.3E-5	-8.0E-7	-1.7E-8

α	β	$E_2(\alpha, \beta)\xi^2$	$E_4(\alpha, \beta)\xi^4$	$E_6(\alpha, \beta)\xi^6$	$E_8(\alpha, \beta)\xi^8$
			$\xi = 0.707$ cont.		
2.0	0.1	-4.0E-1	1.5E-1	-6.0E-2	2.4E-2
	1.0	-1.6E-1	5.1E-3	2.1E-3	-1.6E-4
	2.0	-4.1E-2	-2.1E-3	1.3E-5	8.7E-6
	3.5	-7.9E-3	-3.2E-4	-8.2E-6	-1.1E-7
	5.0	-2.3E-3	-5.8E-5	-1.1E-6	-1.7E-8
5.0	0.1	-2.2E-1	7.0E-2	-2.6E-2	1.0E-2
	1.0	-1.0E-1	4.0E-3	7.8E-4	-6.4E-5
	2.0	-3.8E-2	-5.1E-4	2.0E-5	2.7E-6
	3.5	-1.2E-2	-1.7E-4	-1.2E-6	3.9E-9
	5.0	-5.1E-3	-5.9E-5	-4.1E-7	-1.8E-9

If the coil is to be used as a calibration coil providing a known uniform field then an important factor is the area over which one requires field homogeneity. For example, if the field homogeneity is required over a circular region of 1.0 to 2.0 m diameter, then clearly a large coil is required and in order to minimize weight and costs, it is desirable to minimize α and β. As an example, consider a coil with a radius of 1.0 m, coil thickness of 1 cm ($\alpha = 1.01$) and a length of 20 cm ($\beta = 0.1$). (If $\alpha = 1.5$, then the coil thickness is 50 cm which leads to a massive coil.) The field homogeneity at radial distances away from the centre of the coil, $H_z(\xi, \pi/2)/H_0$, is as large as 7% at a distance of $r = 30$ cm and deteriorates to 23% and 64% at 50 cm and 71 cm away from the coil centre respectively; see Table 4. The final coil dimensions would depend on the required field homogeneity and acceptable tolerances.

Table 4: *Field homogeneity for thin cross-section coils of internal radius 1.0 m*

$\alpha = 1.01$, $\beta = 0.1$ (coil thickness, 1 cm; coil length, 20 cm)

r/a_1	r	$H_z(\xi, \pi/2)/H_0$	$H_z(\gamma, 0)/H_0$
0.3	30 cm	1.071 (+ 7%)	0.882 (- 12%)
0.5	50 cm	1.234 (+ 23%)	0.723 (- 28%)
0.707	71 cm	1.637 (+ 64%)	0.593 (- 41%)

$\alpha = 1.01$, $\beta = 0.4$ (coil thickness, 1 cm; coil length, 80 cm)

r/a_1	r	$H_z(\xi, \pi/2)/H_0$	$H_z(\gamma, 0)/H_0$
0.3	30 cm	1.052 (+ 5%)	0.907 (- 9%)
0.5	50 cm	1.159 (+ 16%)	0.768 (- 23%)
0.707	71 cm	1.366 (+ 37%)	0.602 (- 40%)

2.4 *Hart's Method for Distributed Circular Currents*

Figure 9 depicts a distributed circular current whose positive flow occupies the full rectangular area shown in the shaded region. The coordinates are normalized to the coordinate $P(0, h)$ where h is the perpendicular distance from the z-axis to a point P. For a distributed circular current, Hart [2] obtains the following expression for the radial and axial magnetic fields B_R and B_Z respectively,

$$B_R = kJh \sum_R \sum_Z \sum_\alpha \frac{RZ\cos\alpha(200\,\Delta R\,\Delta Z\,\Delta\alpha)}{[1+R^2+Z^2-2R\cos\alpha]^{3/2}} = kJhS_R \tag{23}$$

$$B_Z = kJh \sum_R \sum_Z \sum_\alpha \frac{(R^2-R\cos\alpha)(200\,\Delta R\,\Delta Z\,\Delta\alpha)}{[1+R^2+Z^2-2R\cos\alpha]^{3/2}} = kJhS_Z \tag{24}$$

where B is in tesla, distance is in metres, J is the current density in A m^{-2} and $k = 10^{-9}$ tesla m A^{-1}. S_R and S_Z apply to a uniform current distribution which occupies the entire shaded rectangular area of Figure 9b from the origin diagonally outward to point Q. *The angular increment* $\Delta\alpha$ was chosen to make $L = \pi/\Delta\alpha$ integral for the semicircle where L is the number of terms in the summation Σ_α. The summation is multiplied by 2 to obtain the required summation around the circle and α is the angle taken to the centre of its corresponding increment. S_R and S_Z are numerical approximations to the intractable triple integrals

$$\int_0^r \int_0^z \int_0^\pi \ldots dr\,dz\,d\alpha$$

which have been evaluated digitally and presented in tabular form for incremental values of Z and R, see Hart's tables I-A, B and C [2]. Unfortunately, four-point interpolation may be necessary to deduce the S_R and S_Z functions at the required R, Z coordinates from the values given in Hart's tables.

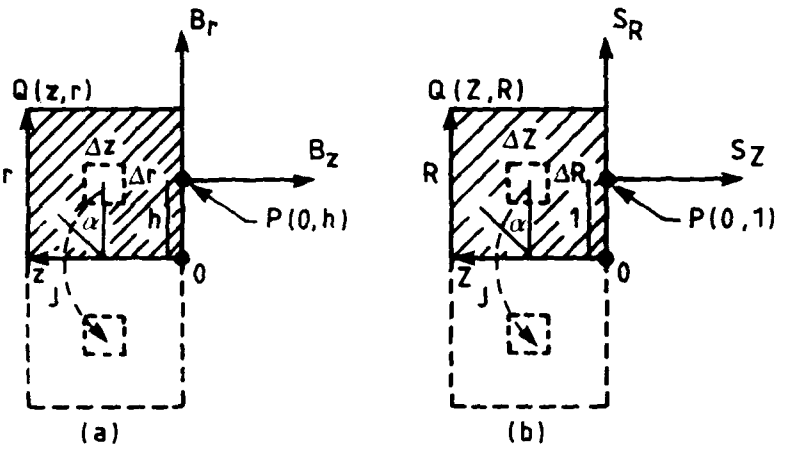

Figure 9: Distributed circular current: (a) dimensionless coordinates, (b) dimensionless coordinates normalized to h, i.e. z = Zh, r = Rh, dz = h dZ and dr = h dR. The origin 0 is taken at the point at which h meets the z-axis.

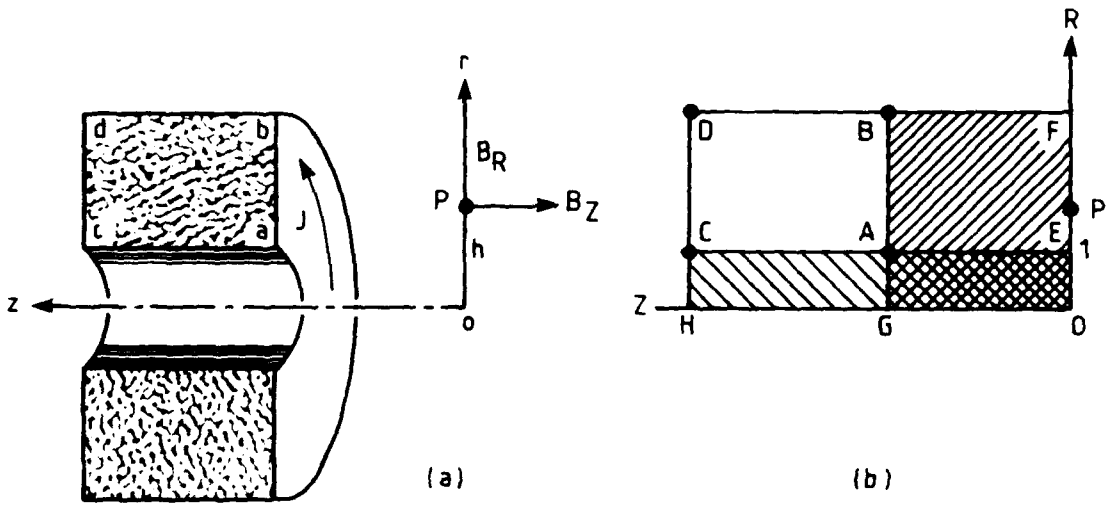

Figure 10: A distributed circular current of rectangular cross section in terms of (a) dimensional coordinates, and (b) normalized coordinates.

For current distributions contained in the typical coil distribution shown in Figure 10a, eqns. 23 and 24 can be modified, (see Fig. 10b), resulting in

$$B_{R,Z} = kJh(S_D - S_B - S_C + S_A)_{R,Z} \tag{25}$$

where the shaded regions in Figure 10b are subtracted from S_D (contribution of area DHOF). However, the contribution from area AGOE has been subtracted twice, resulting in the + S_A term in eqn. 25. Hart's method was used to compute the ratio of the axial field to the central field at various radial distances from the centre of a coil with $\alpha = 1.01$, $\alpha_1 = 100$ cm and coil length $2b = 40$ cm, 100 cm and 200 cm. The results are shown in Figure 11 and a comparison of this technique with Garrett's series expansion approach is summarized in Table 5. The agreement is good except for Hart's value at $h = 30$ cm, $\beta = 0.5$ which is too high. The error associated with this value arises from the two 4-point interpolations required to extract the S_Z integral from Hart's tabulated values. Whilst both techniques give similar results, the series expansion approach is much faster because no numerical integrations are required and the relatively simple $E_n(\alpha, \beta)$ error coefficient functions are readily computed. Accuracy and speed are also improved because there is no need to resort to tables or interpolations. Furthermore, as discussed in the following section, the series expansion approach easily lends itself to the computation of fields from a combination of coaxial coils. Thus the series expansion approach is far superior for numerical modelling studies.

Table 5: Comparison of Hart's numerical integration procedure with Garrett's series expansion method

$H_z(\xi, \pi/2)/H_0$ for a coil $a_1 = 100$ cm, $a_2 = 101$ cm, $\alpha = 1.01$ and coil lengths $2b = 40$ cm ($\beta = 0.2$), 100 cm ($\beta = 0.5$) and 200 cm ($\beta = 1.0$)

	$\beta = 0.2$		$\beta = 0.5$		$\beta = 1.0$	
	Garret	Hart	Garret	Hart	Garret	Hart
$\xi = 0.7$ $h = 70$ cm	1.56	1.55	1.28_6	1.27_9	1.08_9	1.08_7*
$\xi = 0.5$ $h = 50$ cm	1.21_5	1.21_2	1.13_1	1.13_1	1.04_6	1.04_4
$\xi = 0.3$ $h = 30$ cm	1.06_7	1.08_6	1.04_4	1.09_7	1.01_7	1.02_3*

* Obtained by linear interpolation from Figure 11

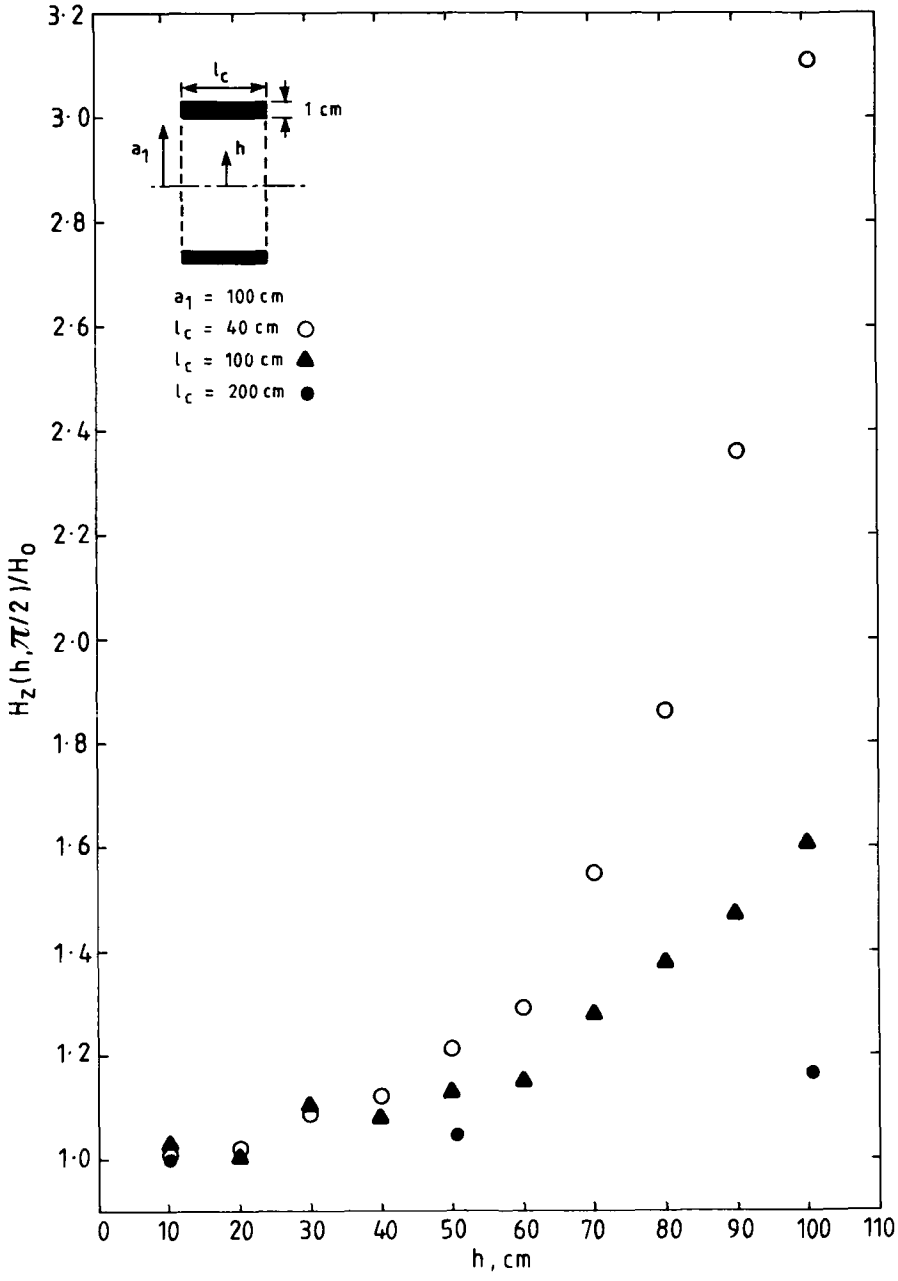

Figure 11: Deviation of axial field $H_z(h, \pi/2)$ from central field H_0 computed from Hart's tables of S_Z functions for coil length 40 cm, 100 cm and 200 cm.

3. *Fields for Two Coaxially Displaced Solenoids*

3.1 *Introduction*

Using the superposition principle and symmetry arguments, the axial field along the coil axis, $H_z(z, 0)$, outside or within a coil or between two or more coils separated by a gap can always be expressed as a sum of central fields. For example, the end field $H_z(z = \beta a_1, 0)$ of any coil is half the central field of a coil twice the length. The field $H_z(\gamma, 0)$ for $\gamma > \beta$, i.e. external to the coil can be computed from the central fields of two sub-coils into which the original coil is partitioned, see Figure 12. Normalized distances are used for the sub-coils. Sub-coil A has geometry $(\alpha, \beta + \gamma)$ and sub-coil B has geometry $(\alpha, \gamma - \beta)$. Thus

$$H_z(\gamma,0) = \frac{H_0^A}{2} - \frac{H_0^B}{2} \tag{26}$$

where from eqn. 11, the central fields of sub-coils A and B are given as

$$\begin{aligned} H_0^A &= j_c \lambda a_1 F(\alpha, \beta + \gamma) \\ H_0^B &= j_c \lambda a_1 F(\alpha, \gamma - \beta) \end{aligned} \tag{27}$$

and thus

$$[H_z(\gamma,0)]_{\gamma>\beta} = H_0 \frac{F(\alpha,\beta+\gamma) - F(\alpha,\gamma-\beta)}{2F(\alpha,\beta)} \tag{28}$$

where H_0 is the central field $H_z(0,0)$ of the original coil with geometry (α, β), i.e. $j_c \lambda a_1 F(\alpha, \beta)$. If the axial field is required at a point along the axis which lies within the coil boundary, then eqn. 10 can be used to modify the term $F(\alpha, \gamma - \beta)$ appearing in eqn. 28, see Figure 13. Thus

$$[H_z(\gamma,0)]_{\gamma<\beta} = H_o \frac{F(\alpha,\beta+\gamma) + F(\alpha,\beta-\gamma)}{2F(\alpha,\beta)}. \tag{29}$$

From eqn. 8, eqns. 28 and 29 reduce to eqn. 19.

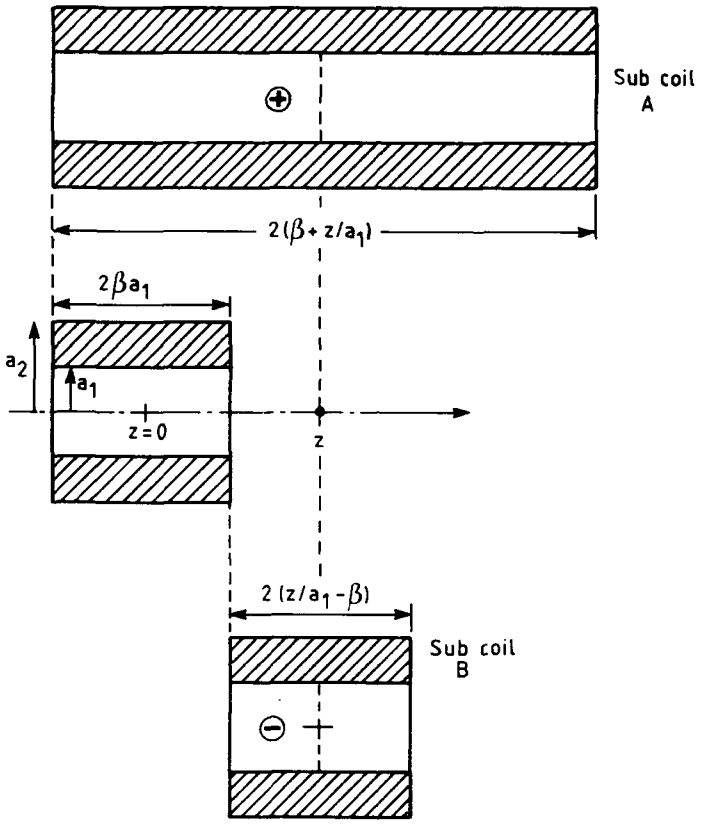

Figure 12: Partitioning of main coil into sub coil A and sub coil B allows the external field $H_z(z, 0)$ to be evaluated from the central field of sub coils A and B. $\gamma = z/a_1$.

3.2 *Axial Fields from Multiple Coils*

The previous analysis by symmetry and superposition arguments can also be applied to more than one coil, for example, a pair of coils [1]. The homogeneity between a pair of coils can then be analysed by the Legendre series expansion technique.

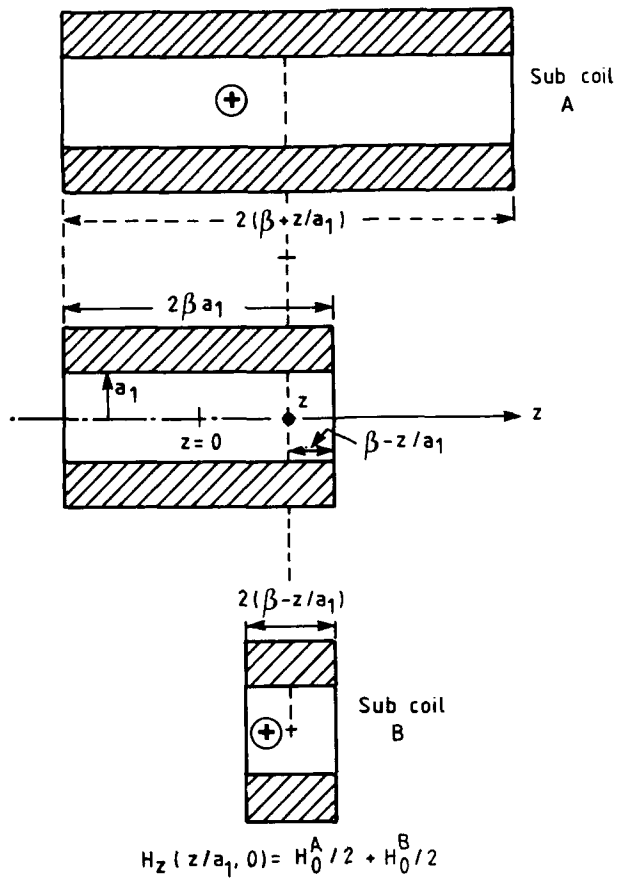

Figure 13: Partitioning of main coil into sub coil A and sub coil B allows the internal field $H_z(z, 0)$ to be evaluated from the central field of sub coils A and B. $\gamma = z/a_1$.

For the pair of coils described in Figure 14, the axial field along the axis is

$$H_z(\gamma,0) = \frac{j_c \lambda a_1}{2} [F(\alpha,2\beta+\beta_g+\gamma) - F(\alpha,\beta_g+\gamma) + F(\alpha,2\beta+\beta_g-\gamma) - F(\alpha,\beta_g-\gamma)] \quad (30)$$

where $\beta_g = g/2a_1$, $F(\alpha, \zeta)$ is defined by eqn. 8 and $H_z(-\gamma, 0) = H_z(\gamma, 0)$. The field at the centre of the gap can then be expressed as

$$H_z(0,0) = j_c \lambda a_1 [F(\alpha, 2\beta + \beta_g) - F(\alpha, \beta_g)] + j_c \lambda a_1 F(\alpha, \beta, \beta_g) \quad (31)$$

Equation 31 is equivalent to a coil of length $4\beta + 2\beta_g$ from which a coil of length $2\beta_g$ has been subtracted.

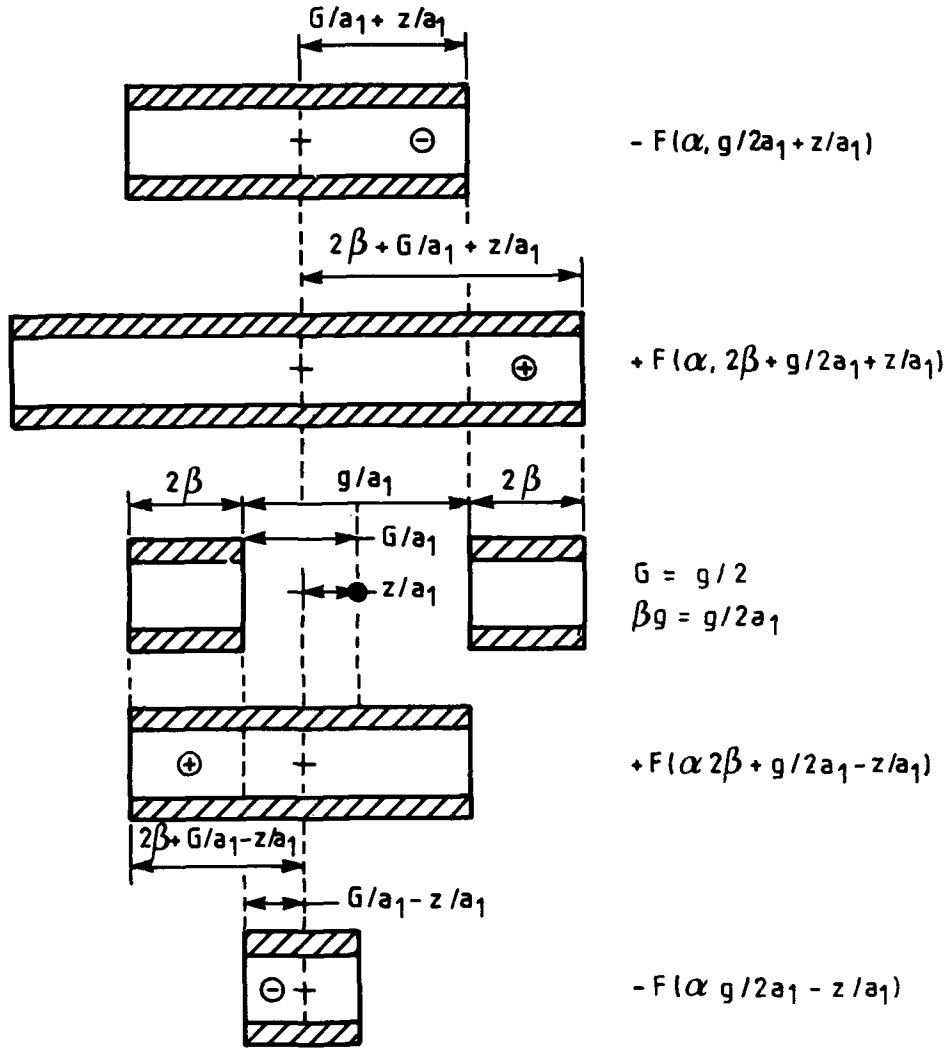

Figure 14: Partitioning of a pair of coaxial coils into four sub coils. $\gamma = z/a_1$.

The deviation of the axial field from the central field, $H_z(\gamma, 0)/H_z(0,0)$, of a split coil pair as one moves away from the centre of the gap can be computed from eqn. 30. The results for a fat coil ($\alpha = 3$, $\beta = 1.0$) and a thin filamentary loop coil ($\alpha = 1.01$, $\beta = 0.1$) are shown in Figures 15, 16 and 17, where the gap width parameter β_g is varied from zero to 2.0 (gap width four times the internal radius). Figures 15 and 16 show two different coils with the same β_g settings. Figure 17 focuses on the homogeneous region of Figure 16. In Figure 15, there are certain gap settings ($\beta \approx 0.25$) where the field homogeneity along the axis is within a few percent of H_0 out to $z/a_1 = 1.0$. A similar result applies to the "filamentary" loop coil, except that the region of field homogeneity holds for a different β_g value and does not extend out to $z/a_1 = 1.0$ as for the fat coil. For example, for the thin foil, Figure 17 reveals that the optimum field homogeneity is obtained at about $\beta_g = 0.45$ up to $z/a_1 = 0.4$ ($H_z(\gamma, 0)/H_0 = 0.9982$). If $\alpha = 1.01$, $\beta = 0.1$ and $a_1 = 100$ cm, then the optimum gap setting is approximately 90 cm and $z = 40$ cm for field homogeneity to within 0.2% of the central field. Figures 15 and 16 also show the axial field deviation for zero gap width. Here the field drops off monotonically away from the coil centre.

The axial field within a region of space around the centre of a single coil is less uniform along the z axis ($\theta = 0$) than radially outwards ($\theta = \pi/2$), see section 2.3 and Table 4. If the same conclusion applied to a pair of coils, then eqn. 30 and Figures 15 to 17 can be used to quantitatively set the upper limits of field homogeneity within a spherical region about the centre of a split coil pair. However this is not always the case and depends on the gap separation and size of coils. Choosing the appropriate β_g for good axial field uniformity along the z axis ($\beta_g = 0.45$, Fig. 17), eqns. 30 and 31 are evaluated and the uniformity $H_z(z/a_1, 0)/H_0$ for certain z/a_1 is shown in Figure 18. (Here the values indicate the percentage deviation from H_0 at r/a_1 and $z/a_1 = 0.3$, 0.4, 0.5, 0.6, 0.8. The deviations in brackets are those obtained from the Legendre expansion technique, see section 3.3). Note that the individual coils ($\alpha = 1.01$, $\beta = 0.1$) are the same as the example given in Table 4 and by comparison, the split coil pair offers better field uniformity by more than an order of magnitude up to $z/a_1 = 0.5$. For example at $z/a_1 = 0.5$, the deviation from the central field is 28% for a single coil compared to 2% for the split coil pair and from Figure 7 at $\alpha = 1.01$, a β value of 1.4 is required to achieve 2% single coil uniformity. This implies a coil length of 2.8 m as opposed to 0.2 m. There are several other interesting features revealed in Figure 18. The Legendre expansion technique which includes terms up to eighth order yields results in excellent agreement with the superposition expressions (eqns. 30 and 31). The discrepancy at larger z/a_1 arises from the contributions of higher order terms. For example, the eighth-order term accounts for 10% of the computed $H_z(\gamma = 0.8, 0)/H_0$ value (0.86480). Another feature is that the field uniformity in the $\theta = \pi/2$ plane is also improved by using a pair of coils rather than a single coil (see Table 4). The field uniformity for the coil pair is better in the z direction than the $\theta = \pi/2$ plane. Similarly, for $\alpha = 3.0$, $\beta = 1.0$ (Fig. 15), the same trend obtains at $\beta_g = 0.2$ but reverses at $\beta_g = 1.0$.

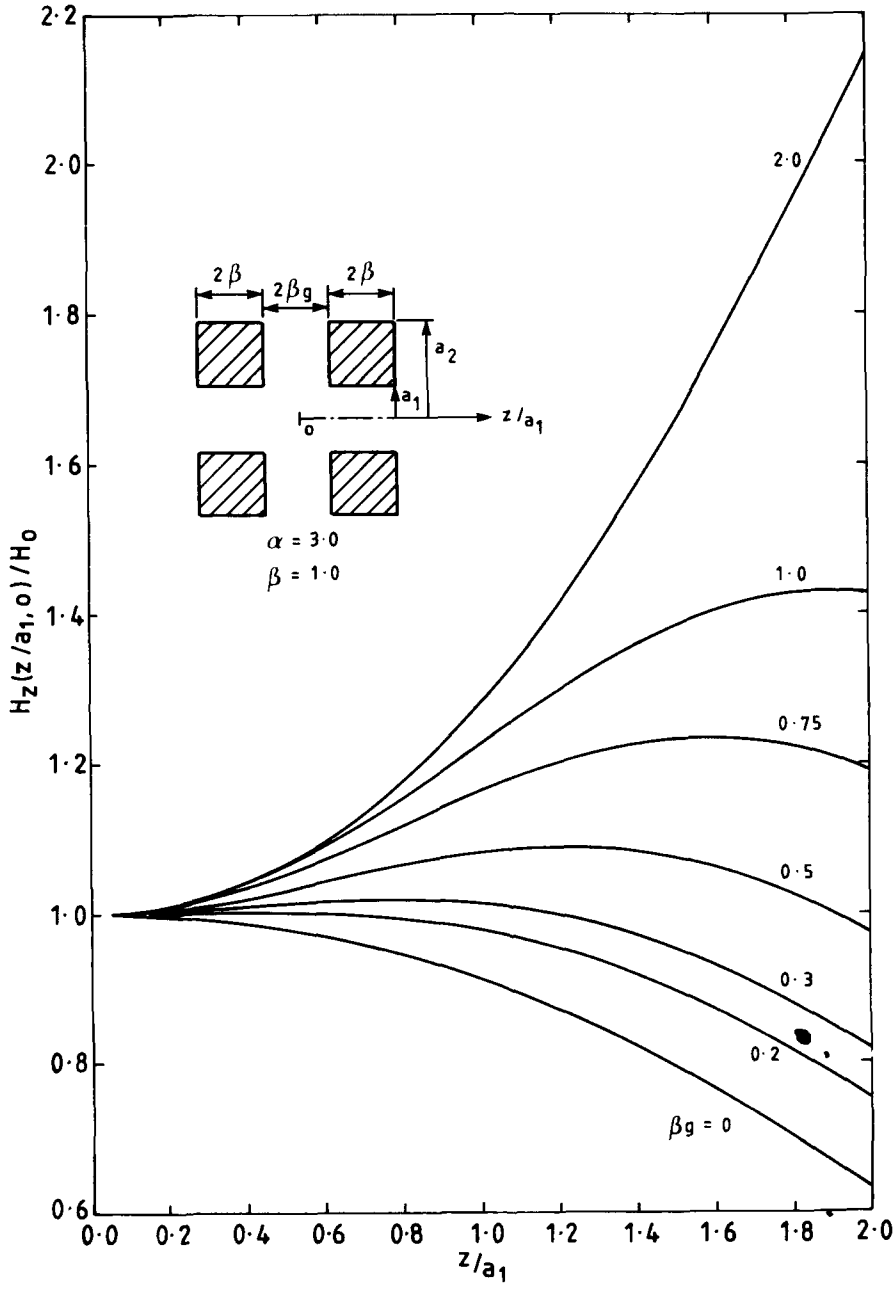

Figure 15: Deviation of axial field $H_z(z/a_1, 0)$ from field at gap centre for a coil pair ($\alpha = 3.0, \beta = 1.0$).

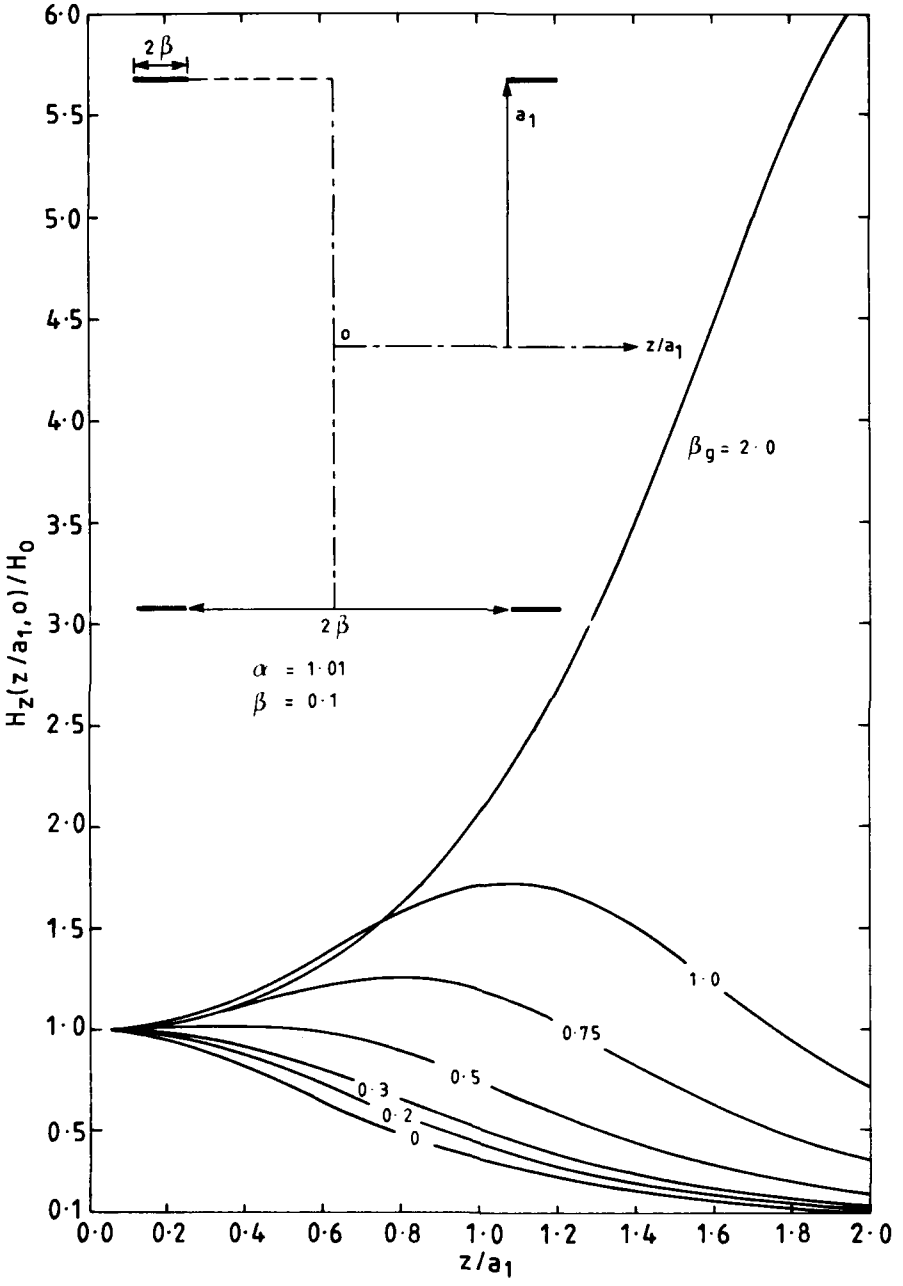

Figure 16: Deviation of axial field $H_z(z/a_1, 0)$ from field at gap centre for a coil pair ($\alpha = 1.01$, $\beta = 0.1$).

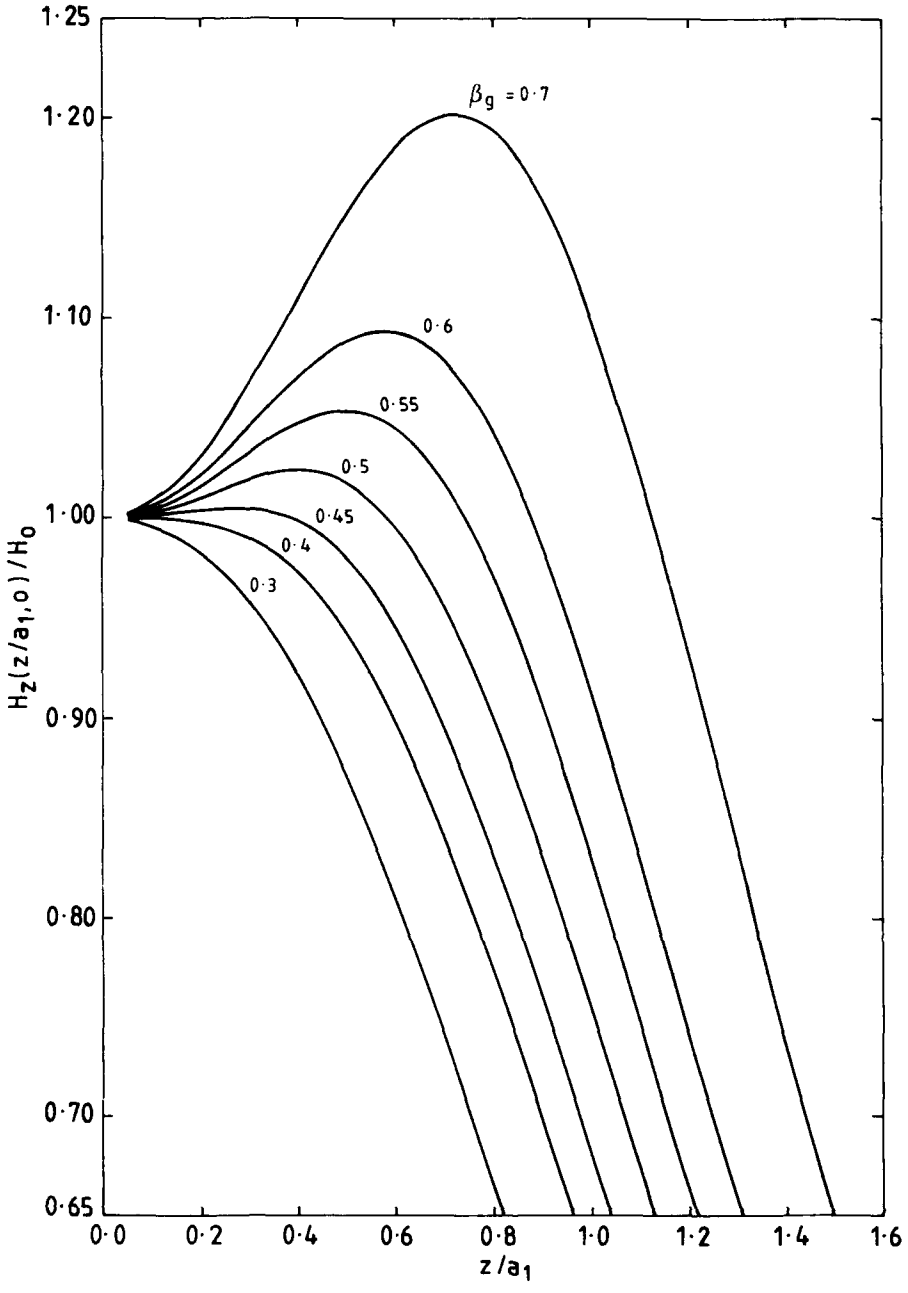

Figure 17: Deviation of axial field $H_z(z/a_1, 0)$ from field at gap centre for a coil pair ($\alpha = 1.01$, $\beta = 0.1$).

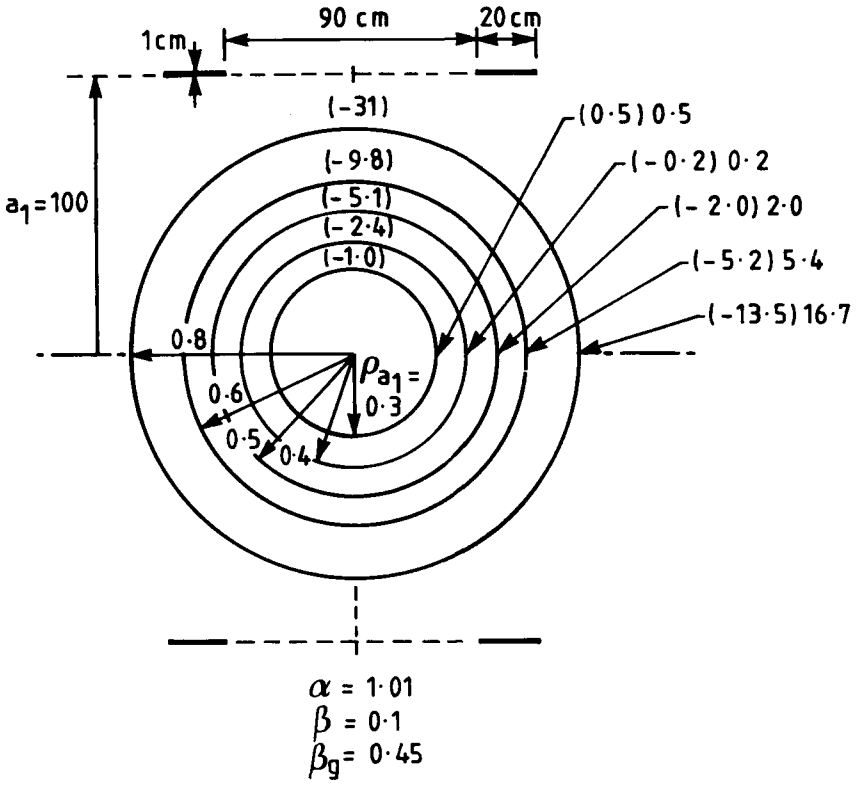

Figure 18: Regions of field uniformity $H_z(\rho/a_1, \theta)/H_0$, $\theta = 0, \pi/2$ for a split coil $\alpha = 1.01$, $\beta = 0.1$, $\beta_g = 0.45$.

3.3 *Fields Within a Central Region for a Pair of Coils*

The Legendre expansion technique is combined with the superposition principle for multiple coils in order to obtain inhomogeneities in the central region of the gap formed by a pair of coaxially displaced coils. Thus the expressions for the axial fields $H_z(\gamma, 0)$ and $H_z(\xi, \pi/2)$, eqns. 20 and 21, will contain for each term a corresponding term representing the compensating coil contribution which for the pair of coils is the imaginary gap or void coil. There is a degree of freedom in choosing the location, inner and outer radius and relative current density of the compensation coil. However, the number of terms in the series expansion of the field generated by the main coil that can be cancelled by the terms arising from the compensating coil is determined by the number of independent variables of the compensating coil. Thus for the separated coil pair in Figure 14, the superimposed "negative" coil produces the gap (upper and lower two sub-coils in Fig. 14) and since the main coil and compensating coil have the same α, the only free variable is β_g, the gap separation.

Consequently, only the $E_2(\alpha, \beta)$ term in the series expansion may be cancelled leading to a fourth-order compensated coil. On the other hand if the main coil is configured to have a notch either on the inside or outside of the coil winding, positioned symmetrically about the mid-plane, then both α_g (≡ the depth of the notch) and β_g (≡ the length of the notch) may be varied. Consequently, both the $E_2(\alpha, \beta)$ and $E_4(\alpha, \beta)$ terms may be cancelled by choosing the appropriate (α_g, β_g) in order to achieve even higher field homogeneities. This configuration leads to a sixth-order compensated coil [6].

Let α, β represent the geometry parameters for the main coil including the gap as shown in Appendix A, (unlike Fig. 14) and let α_g, β_g, refer to the compensating coil (gap). Then, from eqns. 20 and 21,

$$\begin{aligned} H_z(\gamma,0) = j_c\lambda a_1 \Big[& F(\alpha,\beta) - F_g(\alpha_g,\beta_g) \\ & + [F_0E_2(\alpha,\beta) - F_gE_2(\alpha_g,\beta_g)]\gamma^2 \\ & + [F_0E_4(\alpha,\beta) - F_gE_4(\alpha_g,\beta_g)]\gamma^4 \\ & + [F_0E_6(\alpha,\beta) - F_gE_6(\alpha_g,\beta_g)]\gamma^6 \\ & + [F_0E_8(\alpha,\beta) - F_gE_8(\alpha_g,\beta_g)]\gamma^8 \\ & + \ldots \Big), \end{aligned} \tag{32}$$

$$\begin{aligned} H_z(\xi,\pi/2) = j_c\lambda a_1 \Big[& F(\alpha,\beta) - F_g(\alpha_g,\beta_g) \\ & - \frac{1}{2}[F_0E_2(\alpha,\beta) - F_gE_2(\alpha_g,\beta_g)]\xi^2 \\ & + \frac{3}{8}[F_0E_4(\alpha,\beta) - F_gE_4(\alpha_g,\beta_g)]\xi^4 \\ & - \frac{5}{16}[F_0E_6(\alpha,\beta) - F_gE_6(\alpha_g,\beta_g)]\xi^6 \\ & + \frac{35}{128}[F_0E_8(\alpha,\beta) - F_gE_8(\alpha_g,\beta_g)]\xi^8 \\ & + \ldots \Big) \end{aligned} \tag{33}$$

where $F_iE_n(\alpha_i, \beta_i)$ is the product of the field factor (eqn. 8) and eqn. 18 (see Table 2) both evaluated at α_i, β_i. If $F_0E_2(\alpha, \beta) = F_gE_2(\alpha_g, \beta_g)$, the main coil will be compensated to fourth order. This defines a Helmholtz coil pair.

A graphical and hence approximate solution can be obtained by plotting $FE_2(\alpha, \beta)$ as a function of β for various values of α. The results are shown in Figures 19 to 22 which can be readily used for determining the correct gap widths. The expanded left hand portion of Figures 19 and 21 appear in Figures 20 and 22 respectively and are required for determining the correct β_g value for fourth order compensation. For example, for $\alpha = 3$, $\beta = 2$, $FE_2(3, 2) = -0.153 \approx FE_2(3, 0.193)$; thus a gap setting $\beta_g = 0.193$ will yield the maximum central homogeneity. It is evident from Figures 19 to 22 that for a given α, the further away that β is from the minimum of the $FE_2(\alpha, \beta)$ curve, then the smaller the required β_g value for fourth-order compensation. This leads to *fat* coils with a narrow spacing ($\beta_g << \beta$) coils. On the other hand, if β

is chosen close to the minimum then β_g is a large proportion of β and this configuration gives rise to *thin* pancake-type coils which are lighter and more economical than the fat ($\beta_g << \beta$) coils. As an example, let $\alpha = 1.01$ and $a_1 = 100$ cm. When $\beta = 1.0$, $FE_2(\alpha, \beta) = -6.63 \times 10^{-3}$ and from Figure 22, β_g is 0.20, $FE_2(\alpha, \beta_g) = -6.65 \times 10^{-3}$; this leads to the coil configuration shown in Figure 23a. If, however, $\beta = 0.65$, $FE_2(\alpha, \beta_g) = -1.00 \times 10^{-2}$ then $\beta_g = 0.39$ and one obtains the configuration described in Figure 23b.

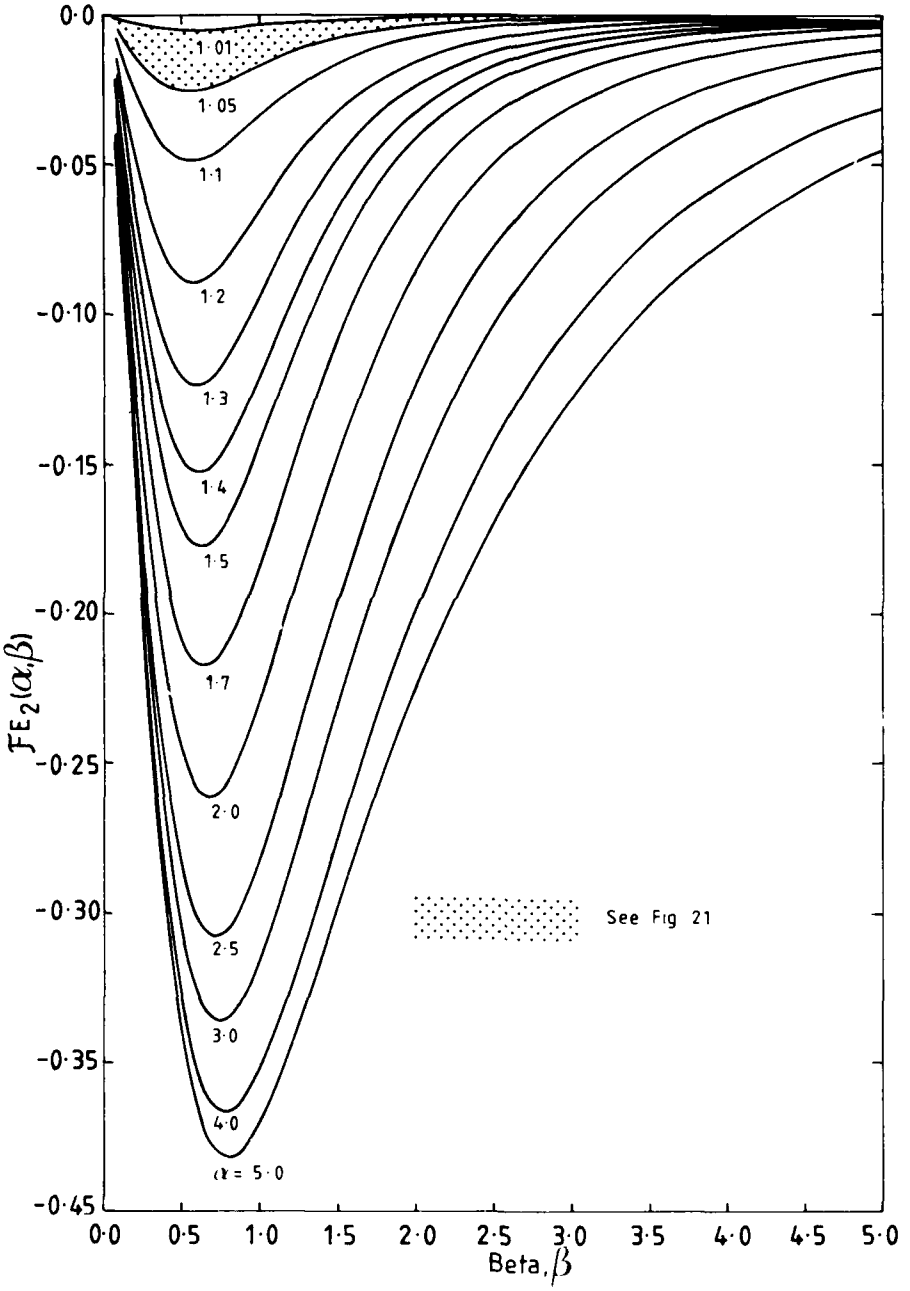

Figure 19: $FE_2(\alpha, \beta)$ as a function of β for $\alpha = 1.01, 1.05, 1.1, 1.2, 1.3, 1.4, 1.5, 1.7, 2.0, 2.5, 3.0, 4.0$ and 5.0.

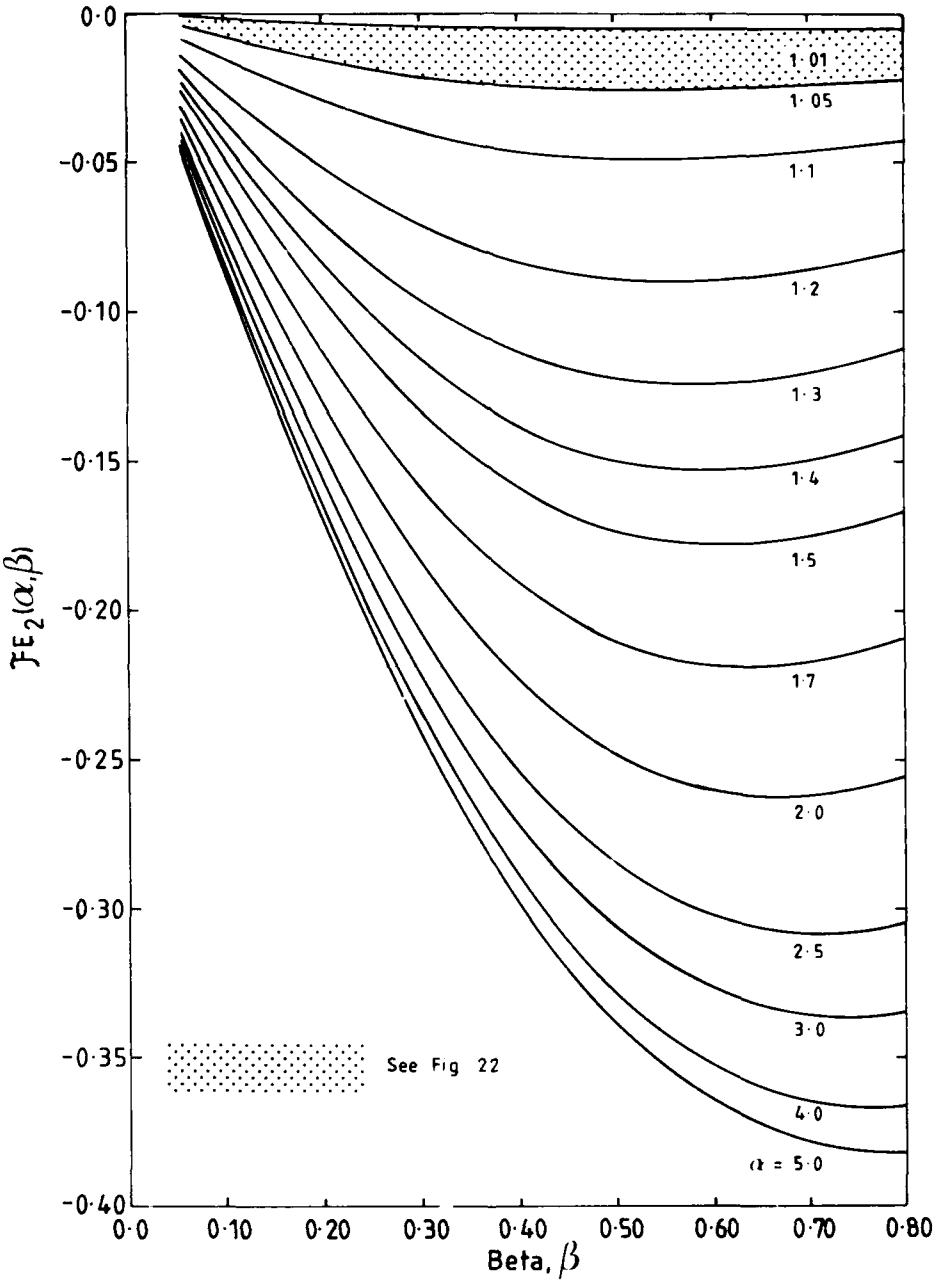

Figure 20: Expanded portion of Figure 19.

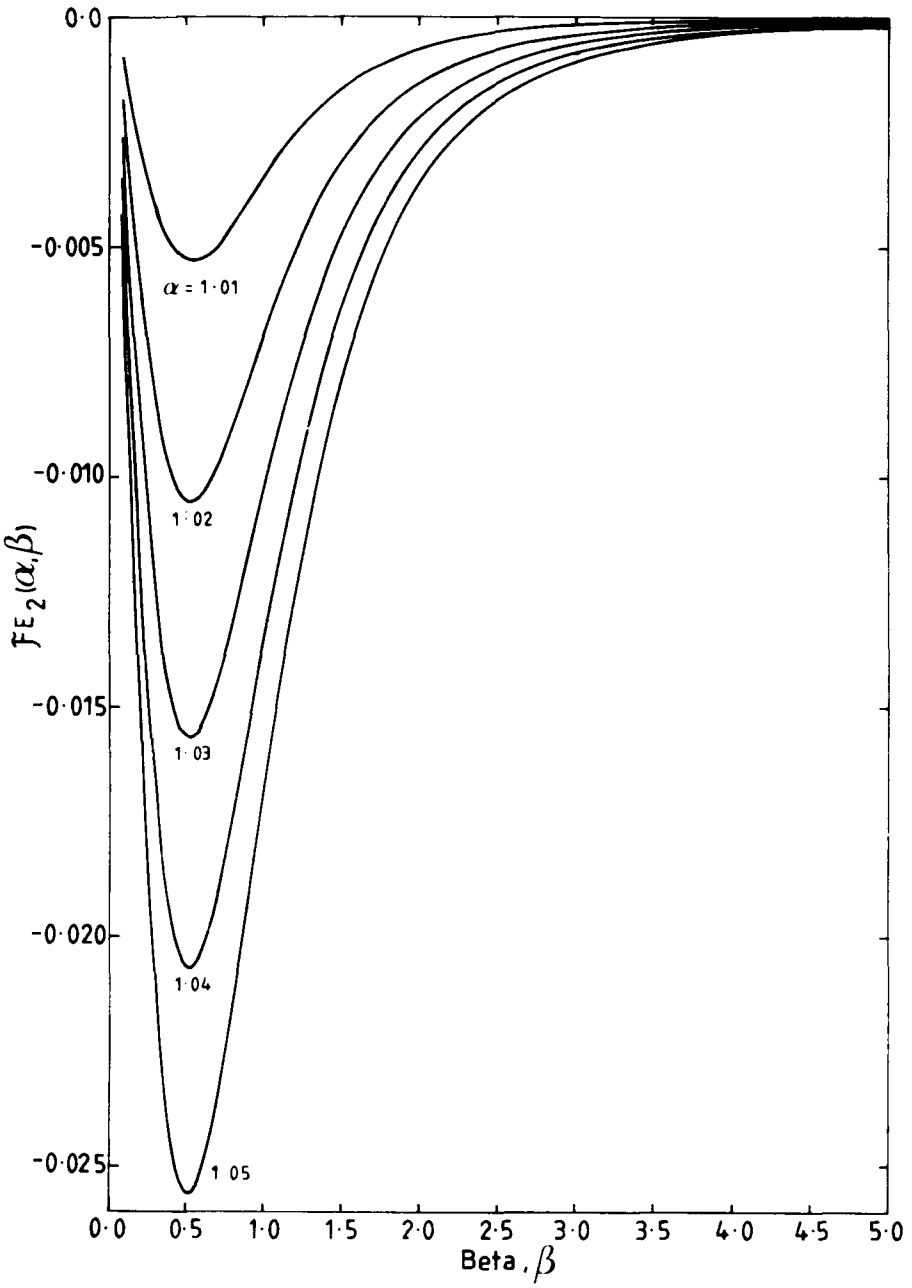

Figure 21: $FE_2(\alpha, \beta)$ as a function of β for α = 1.01, 1.02, 1.03, 1.04 and 1.05.

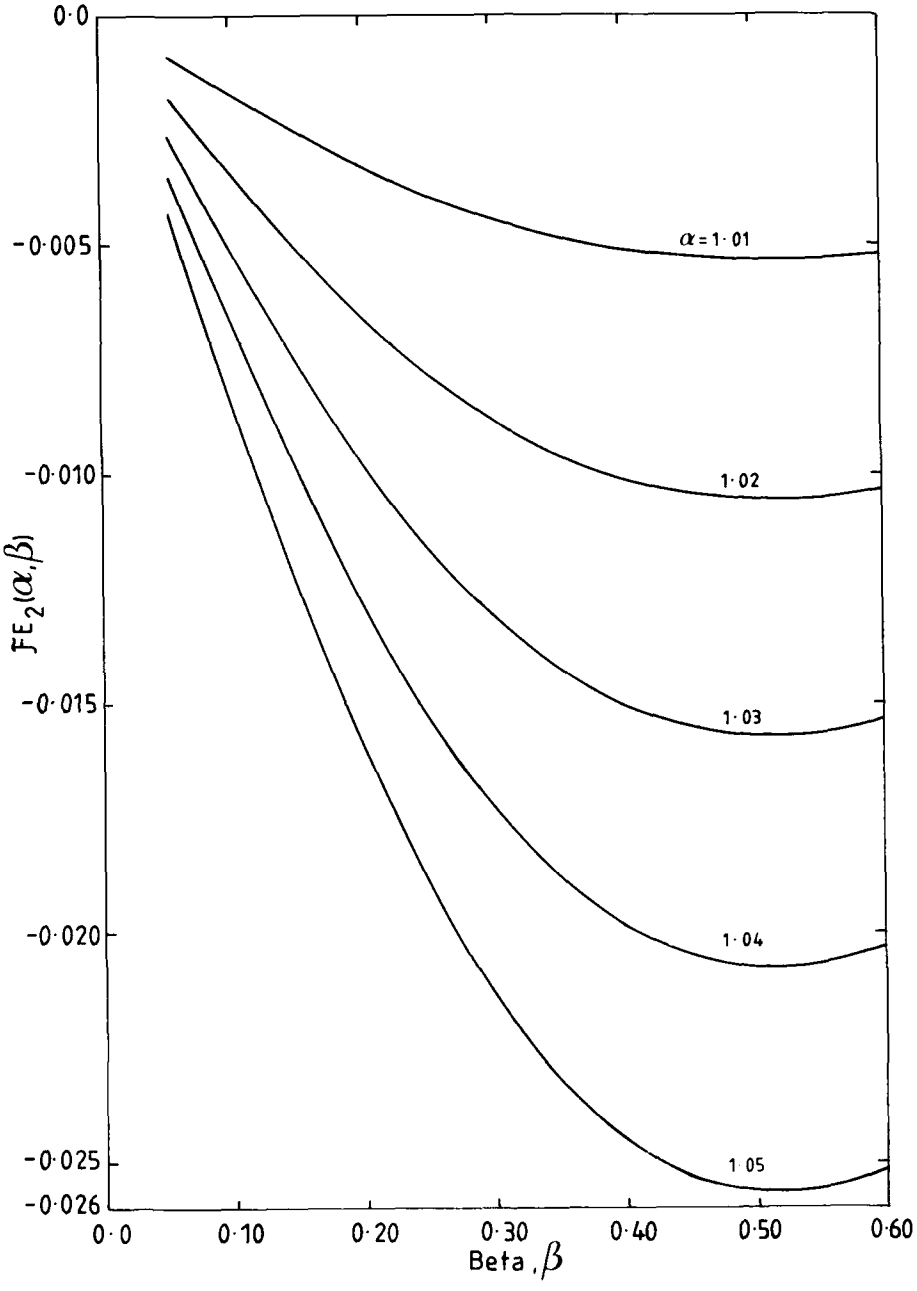

Figure 22: Expanded portion of Figure 21.

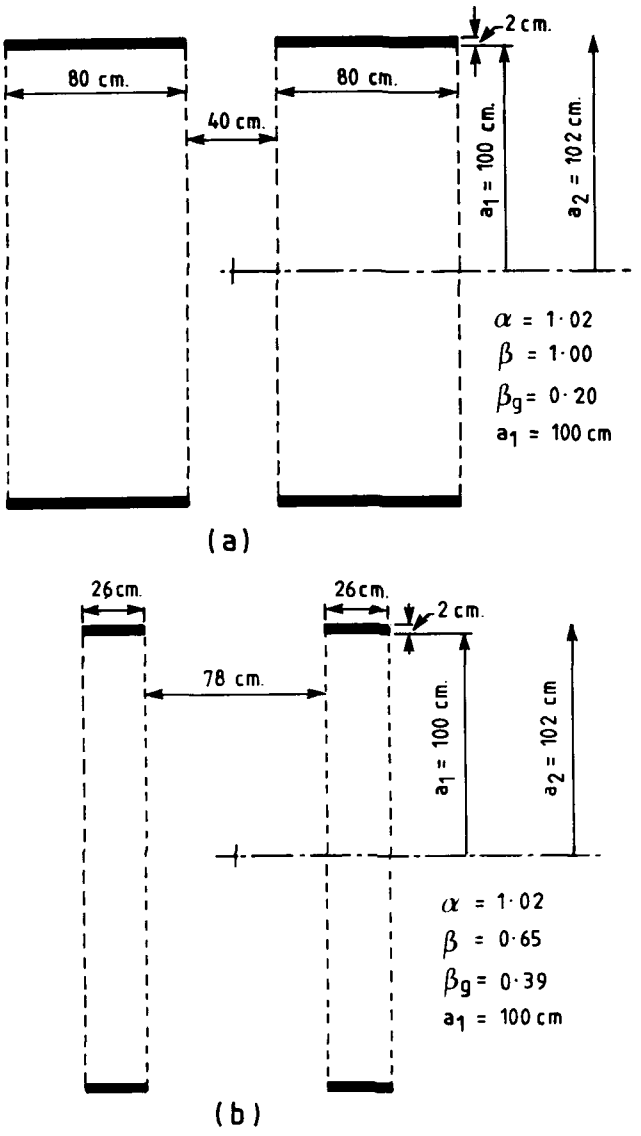

Figure 23: Fourth order compensated coils (scale 1:32).

Another interesting feature displayed by Figures 19 and 21 is that for small values of α (≤ 1.2) the minimum $FE_2(\alpha, \beta)$ value occurs at $\beta \approx 0.5$. Correct compensation at the $FE_2(\alpha, \beta)$ minimum implies $\beta_g \approx \beta$. This leads to the approximate result that for Helmholtz coils, the gap width is equal to the internal radius of short coils. As α increases, the $FE_2(\alpha, \beta)$ minimum occurs at larger β values. At $\alpha = 5.0$, the $FE_2(\alpha, \beta)$ minimum obtains at $\beta = 0.8$ ($\beta_g \approx \beta$) and the required gap width for Helmholtz coils is $1.6a_1$. Figures 19 and 21 are also useful for determining the minimum values of β for a given α to allow for fourth-order compensation. If $\beta \leq 0.8$ for a coil having $\alpha = 5.0$, then fourth-order compensation is not possible.

3.4 *Numerical Computation of Compensated Fourth Order Coils*

In the previous section, computer generated plots were used to provide graphical solutions for choosing the coil parameters β and β_g for a given α. However, it is also useful to automatically compute the correct coil parameters for obtaining compensated coils. This allows a more comprehensive study to be undertaken and is also useful for tabulating error limit tables (see section 3.5).

3.4.1 *The Newton-Raphson Method for Determining* β_g

To compute $H_z(\gamma, 0)$ and $H_z(\xi, \pi/2)$ (eqns. 32, 33) to fourth-order, it is necessary to solve (see Table 2)

$$\frac{1}{2\beta}\left(\frac{1}{(1+\beta^2)^{3/2}} - \left[\frac{\alpha^2}{\alpha^2+\beta^2}\right]^{3/2}\right) = \frac{1}{2\beta_g}\left(\frac{1}{(1+\beta_g^2)^{3/2}} - \left[\frac{\alpha_g^2}{\alpha_g^2+\beta_g^2}\right]^{3/2}\right) \tag{34}$$

for β_g in terms of α and β ($\alpha = \alpha_g$ for Helmholtz coils). Equation 34 cannot be solved analytically and so must be solved numerically using, for example, the Newton Raphson technique for the solution of nonlinear equations [7]. This technique is well-suited to this case because the derivative of the function can be expressed analytically. However, because of the geometry of the method, the Newton-Raphson method can be erratic in regions where the function has a small slope.

The Newton-Raphson method attempts the solution of the equation $F(x) = 0$ where if x_i is an approximation to x, then a better approximation is

$$x_{i+1} = x_i - \frac{F(x_i)}{F'(x_i)} \tag{35}$$

or

$$\Delta x_i F'(x_i) + F(x_i) = 0 \tag{36}$$

where $F'(x_i)$ is the first derivative of $F(x_i)$, in this case, $F_0E_2(\alpha, \beta) - F_gE_2(\alpha_g, \beta_g)$. If Δx_i ($= x_{i+1} - x_i$) is less than a given tolerance, i.e. Δx_i approaches zero, then x_i is an approximate solution.

3.5 *Error Limits for Helmholtz Coils*

As pointed out previously, the terms in eqns. 16 and 17 have their largest value when $\theta = 0$, $P_n(1) = 1$, and the maximum value of the terms for the axial field is given by eqn. 20 or 32. When the second term in eqn. 32 is zero, there remains only the fourth order term and the deviation from the central field H_z/H_0 is

$$H_z(\gamma,0) = 1 + \left(\frac{F_0 E_4(\alpha,\beta) - F_g E_4(\alpha,\beta_g)}{F_0(\alpha,\beta) - F_g(\alpha,\beta_g)} \right) \gamma^4 = 1 + A\gamma^4 + \ldots \tag{37}$$

where

$$H_0 = j_c \lambda a_1 [F_0(\alpha,\beta) - F_g(\alpha,\beta_g)] \tag{38}$$

and if Δ is the percentage change in $H_z(\gamma, 0)$ from H_0 then

$$\frac{z}{a_1} = \left(\frac{\Delta}{100A} \right)^{1/4} \tag{39}$$

determines how far from the origin one can move before the field deviates by more than a given percentage Δ. This assumes that sixth-order and higher contributions are negligible. The evaluation of z/a_1 in eqn. 39 is readily determined using the Newton-Raphson method to automatically compute the required β_g for cancellation of the second order term. Some sample computations for "short" and "long" coil pairs are presented in Table 6. Thus, depending upon the acceptable errors, a significant portion of the coil may be used to provide an approximately uniform magnetic field for calibration purposes.

Table 6: Axial field error limits for fourth-order coils

					z/a_1**		
α	β	β_g	ℓ*/cm	ℓ_g*/cm	0.1%	1.0%	5.0%
1.01	1.0	0.197	200	39.4	0.201	0.357	0.534
	0.6	0.415	120	83	0.174	0.309	0.463
1.03	1.0	0.202	200	40.4	0.202	0.359	0.537
	0.6	0.424	120	84.8	0.173	0.312	0.467
1.05	1.0	0.207	200	41.4	0.203	0.361	0.540
	0.6	0.433	120	86.6	0.173	0.315	0.471
1.1	1.0	0.221	200	44.2	0.206	0.366	0.547
	0.6	0.454	120	90.8	0.181	0.322	0.481
1.5	1.2	0.236	240	47.2	0.241	0.428	0.640
	0.8	0.433	160	86.6	0.212	0.377	0.564
2.0	1.3	0.279	260	55.8	0.265	0.472	0.706
	0.8	0.543	160	108.6	0.234	0.416	0.623
4.0	1.5	0.363	300	72.6	0.321	0.571	0.853
	0.9	0.666	180	133.2	0.288	0.513	0.767

* ℓ and ℓ_g refer to overall coil length including gap, and gap width respectively for an inner radius of 100 cm.

** z/a_1 determines how far from the origin one can move before the field deviates by more than the given percentage.

3.6 *Axial Fields for Uncompensated Coil Pairs*

As shown in Figures 15 to 17, it is possible to forgo maximum field homogeneity for the sake of extending z/a_1 such that the deviation from the central field is within certain error limits. For example, the $\beta_g = 0.45$ curve in Figure 17 extends further out than the $\beta_g = 0.4$ curve, etc. It is thus desirable to evaluate $H_z(\gamma, 0)$ and $H_z(\xi, \pi/2)$ for a coil pair when the second-order term has not been cancelled out, i.e. evaluate eqns. 32 and 33. A Fortran source code listing for the evaluation of these equations is described briefly in Appendix A; the programme also generates two plot files for graphing $H_z(\gamma, 0)/H_0$ and $H_z(\xi, \pi/0)/H_0$ and a scratch file listing the second-, fourth-, sixth- and eighth-order contributions so that the convergence of eqns. 32 and 33 can be monitored. Thus one can readily examine the deviation of the axial field from the central field, both radially and along the z-axis, for a range of β_g values, including the one required for fourth-order compensation.

3.6.1 *Experimental Design Example*

As an example, consider a split coil with two adjustable lengths where $\alpha = 1.01$ and $\beta = 0.50$ and 0.55. The computed axial field deviations $H_z(z/a_1, 0)/H_0$ and $H_z(r/a_1, \pi/2)/H_0$ for various gap settings are shown in Figures 24 and 25. As is evident from these graphs, as β_g approaches 0.5, the correct fourth-order compensation coil setting, better field homogeneity is obtained. With regards to $H_z(r/a_1, \pi/2)/H_0$, it is also clear from these figures that other values of β_g still give a very small deviation (albeit a larger one) from the central field at far greater displacements from the gap centre. There is also very little variation between the results shown in Figures 24 and 25 and those obtained from $\alpha = 1.005$, 1.02 and 1.03 which suggests that it is advantageous to use coils with small α to allow for easier winding and less overall weight. The use of low α values becomes important when field homogeneity is required over a large area.

In Figure 24, the axial field $H_z(r/a_1, \pi/2)$ at $\beta_g = 0.35$ does not deviate by more than 1% from H_0 for displacements of up to 60% of the internal radius of the coils. The axial field $H_z(z/a_1, 0)$ is also uniform to within 1% of H_0 for displacements of up to $0.15a_1$ each way along the z-axis. Thus for a standard internal radius of 100 cm the field is expected to be uniform to within 1% of H_0 for a region of space bounded by a disc (sensor coil) having a radius of 60 cm and a thickness of 30 cm. This was verified experimentally. If better field uniformity is required over a smaller region of space, then one can increase the size of the gap using the original pair of coils (see Fig. 25) where β has now been increased from 0.5 to 0.55 and $\beta_g = 0.40$. Now, $H_z(r/a_1, \pi/2)$ $[H_z(z/a_1, 0)]$ is uniform to within 0.2% of H_0 for displacements up to $r/a_1 = 0.4$ $[z/a_1 = 0.1]$. Tables 7 and 8 contain the information presented in Figures 24 and 25 in tabular form to allow for better quantitative estimates of field uniformity as these coil configurations will be used experimentally.

The accuracy of the uniformity can be checked from the convergence of the series expansion given by eqns. 32 and 33. The even error coefficients $F_0E_n(\alpha, \beta) - F_gE_n(\alpha, \beta_g)$ up to eighth order for the coaxially displaced coil pairs given in Figures 24 and 25 are presented in Table 9 for $\beta_g = 0.35$, $\beta = 0.5$ and $\beta_g = 0.4$, $\beta = 0.55$. For $\alpha = 1.01$, $\beta = 0.55$, $\beta_g = 0.4$, the results in Table 9 show that up to $r/a_1 = 0.4$ the series has converged rapidly and that it is not necessary to go beyond the fourth-order term. On the other hand, for $\alpha = 1.01$, $\beta = 0.5$, $\beta_g = 0.35$ it is necessary to go beyond the fourth-order term to obtain convergence for $r/a_1 \leq 0.65$, $z/a_1 \leq 0.65$. From Table 7, $H_z(0.65, \pi/2) = 0.97\ H_0$ and from eqn. 33 and Table 9, the eighth-order contribution is 0.98% of the total $H_z(0.65, \pi/2/H_0$. Since higher order terms contribute less, the uniformity of $H_z(r/a_1, \pi/2)/H_0$ to better than 3%, for r/a_1 up to 0.65, is not affected by truncating the series at the eighth-order term.

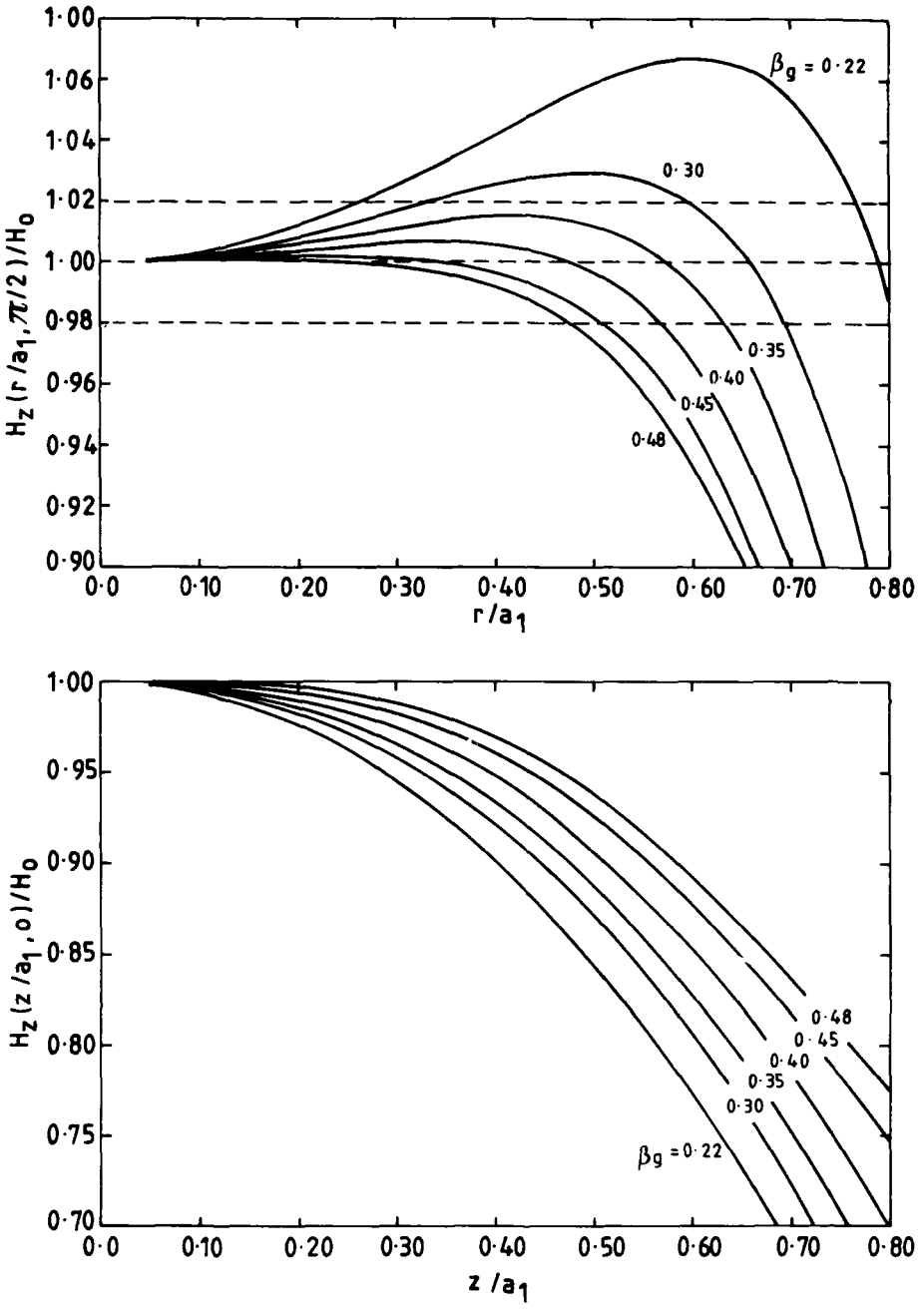

Figure 24: Deviation of axial fields $H_z(r/a_1, \pi/2)$ and $H_z(z/a_1, 0)$ from the central field H_0 for a coil pair: $\alpha = 1.01$, $\beta = 0.50$ and $\beta_g = 0.48, 0.45, 0.40, 0.35, 0.3$ and 0.22.

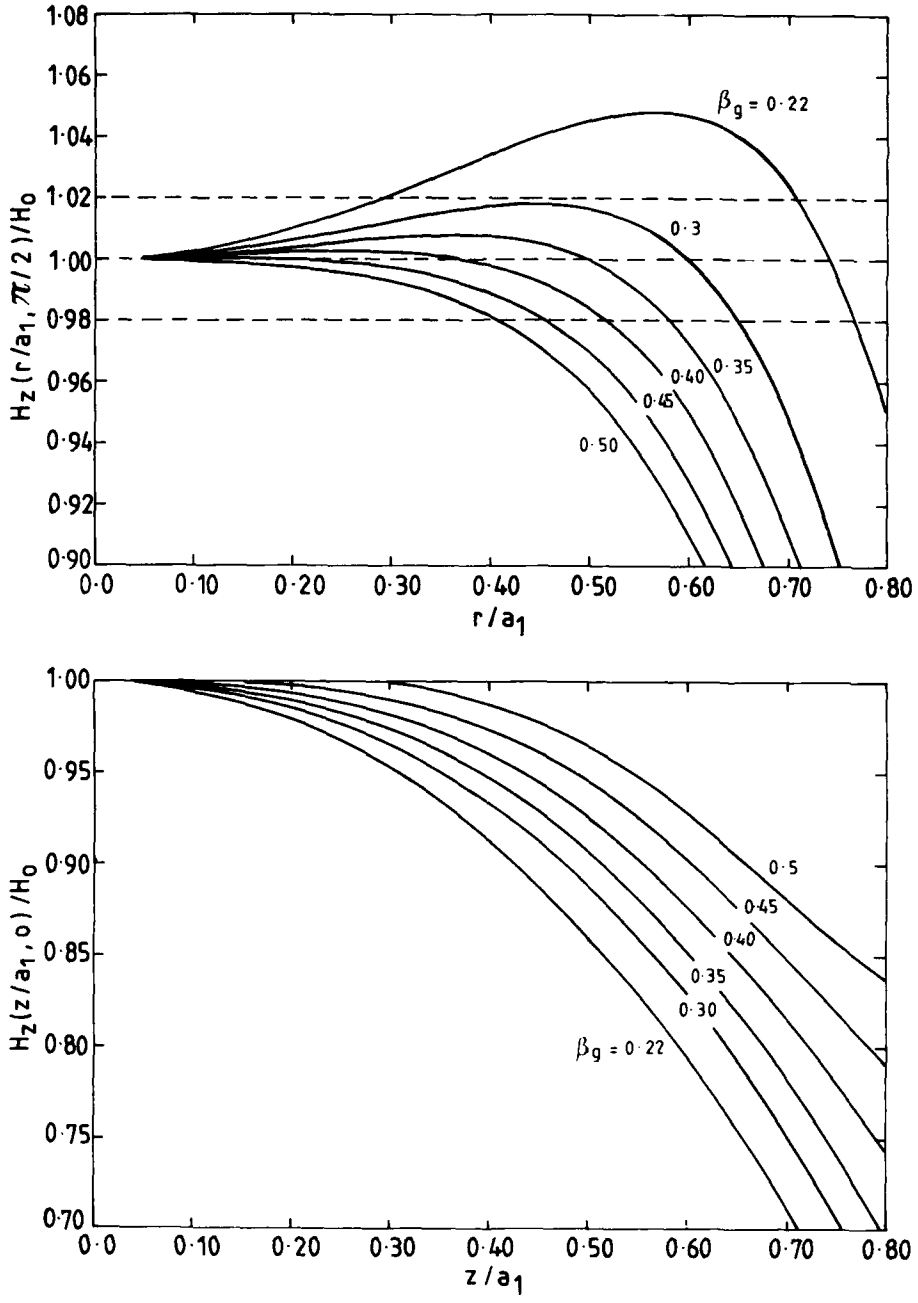

Figure 25: Deviation of axial fields $H_z(r/a_1, \pi/2)$ and $H_z(z/a_1, 0)$ from the central field H_0 for a coil pair: $\alpha = 1.01$, $\beta = 0.55$ and $\beta_g = 0.50, 0.45, 0.40, 0.35, 0.3$ and 0.22.

Table 7: Axial field deviations from the central field at various gap settings for $\alpha = 1.01, \beta = 0.50$

$H_z(r/a_1, \pi/2)/H_0$

$\beta_g = 0.48$	$\beta_g = 0.45$	$\beta_g = 0.40$	$\beta_g = 0.35$	$\beta_g = 0.30$	$\beta_g = 0.22$	r/a_1
1.0001E+00	1.0001E+00	1.0003E+00	1.0004E+00	1.0005E+00	1.0007E+00	0.05
1.0002E+00	1.0005E+00	1.0010E+00	1.0015E+00	1.0021E+00	1.0029E+00	0.10
1.0003E+00	1.0010E+00	1.0022E+00	1.0034E+00	1.0046E+00	1.0065E+00	0.15
1.0003E+00	1.0015E+00	1.0036E+00	1.0058E+00	1.0080E+00	1.0115E+00	0.20
9.9979E-01	1.0017E+00	1.0050E+00	1.0085E+00	1.0121E+00	1.0177E+00	0.25
9.9852E-01	1.0013E+00	1.0062E+00	1.0113E+00	1.0166E+00	1.0251E+00	0.30
9.9599E-01	9.9985E-01	1.0066E+00	1.0138E+00	1.0212E+00	1.0333E+00	0.35
9.9158E-01	9.9668E-01	1.0057E+00	1.0154E+00	1.0255E+00	1.0420E+00	0.40
9.8444E-01	9.9097E-01	1.0026E+00	1.0152E+00	1.0286E+00	1.0508E+00	0.45
9.7352E-01	9.8164E-01	9.9631E-01	1.0123E+00	1.0295E+00	1.0587E+00	0.50
9.5745E-01	9.6726E-01	9.8524E-01	1.0052E+00	1.0270E+00	1.0647E+00	0.55
9.3446E-01	9.4602E-01	9.6753E-01	9.9192E-01	1.0191E+00	1.0674E+00	0.60
9.0237E-01	9.1558E-01	9.4069E-01	9.6991E-01	1.0033E+00	1.0644E+00	0.65
8.5837E-01	8.7297E-01	9.0147E-01	9.3577E-01	9.7624E-01	1.0530E+00	0.70
7.9901E-01	8.1443E-01	8.4573E-01	8.8511E-01	9.3345E-01	1.0292E+00	0.75
7.1997E-01	7.3526E-01	7.6816E-01	8.1221E-01	8.6912E-01	9.8770E-01	0.80
6.1591E-01	6.2958E-01	6.6207E-01	7.0979E-01	7.7574E-01	9.2180E-01	0.85
4.8031E-01	4.9010E-01	5.1903E-01	5.6857E-01	6.4365E-01	8.2257E-01	0.90
3.0518E-01	3.0786E-01	3.2855E-01	3.7688E-01	4.6063E-01	6.7863E-01	0.95
8.0824E-02	7.1856E-02	7.7606E-02	1.2014E-01	2.1128E-01	4.7554E-01	1.00

$H_z(z/a_1, 0)/H_0$

$\beta_g = 0.48$	$\beta_g = 0.45$	$\beta_g = 0.40$	$\beta_g = 0.35$	$\beta_g = 0.30$	$\beta_g = 0.22$	z/a_1
9.9987E-01	9.9973E-01	9.9947E-01	9.9921E-01	9.9895E-01	9.9853E-01	0.05
9.9941E-01	9.9883E-01	9.9782E-01	9.9678E-01	9.9574E-01	9.9410E-01	0.10
9.9838E-01	9.9708E-01	9.9484E-01	9.9255E-01	9.9024E-01	9.8664E-01	0.15
9.9641E-01	9.9413E-01	9.9023E-01	9.8624E-01	9.8226E-01	9.7606E-01	0.20
9.9303E-01	9.8954E-01	9.8359E-01	9.7756E-01	9.7154E-01	9.6226E-01	0.25
9.8772E-01	9.8282E-01	9.7453E-01	9.6616E-01	9.5787E-01	9.4516E-01	0.30
9.7993E-01	9.7349E-01	9.6263E-01	9.5176E-01	9.4105E-01	9.2475E-01	0.35
9.6920E-01	9.6112E-01	9.4757E-01	9.3410E-01	9.2093E-01	9.0105E-01	0.40
9.5516E-01	9.4540E-01	9.2912E-01	9.1305E-01	8.9746E-01	8.7413E-01	0.45
9.3760E-01	9.2615E-01	9.0716E-01	8.8854E-01	8.7060E-01	8.4406E-01	0.50
9.1653E-01	9.0339E-01	8.8169E-01	8.6052E-01	8.4028E-01	8.1075E-01	0.55
8.9218E-01	8.7730E-01	8.5274E-01	8.2889E-01	8.0625E-01	7.7386E-01	0.60
8.6502E-01	8.4819E-01	8.2033E-01	7.9329E-01	7.6785E-01	7.3245E-01	0.65
8.3573E-01	8.1642E-01	7.8423E-01	7.5289E-01	7.2367E-01	6.8465E-01	0.70
8.0511E-01	7.8228E-01	7.4372E-01	7.0595E-01	6.7110E-01	6.2713E-01	0.75
7.7398E-01	7.4576E-01	6.9727E-01	6.4937E-01	6.0574E-01	5.5446E-01	0.80
7.4298E-01	7.0626E-01	6.4201E-01	5.7805E-01	5.2057E-01	4.5820E-01	0.85
7.1235E-01	6.6220E-01	5.7313E-01	4.8399E-01	4.0497E-01	3.2587E-01	0.90
6.8153E-01	6.1054E-01	4.8312E-01	3.5532E-01	2.4350E-01	1.3962E-01	0.95
6.4881E-01	5.4614E-01	3.6078E-01	1.7499E-01	1.4403E-02	-1.2537E-01	1.00

Table 8: Axial field deviations from the central field at various gap settings for $\alpha = 1.01, \beta = 0.55$

$H_z(r/a_1, \pi/2)/H_0$

$\beta_g = 0.50$	$\beta_g = 0.45$	$\beta_g = 0.40$	$\beta_g = 0.35$	$\beta_g = 0.30$	$\beta_g = 0.22$	r/a_1
9.9989E-01	1.0000E+00	1.0001E+00	1.0003E+00	1.0004E+00	1.0006E+00	0.05
9.9954E-01	1.0000E+00	1.0005E+00	1.0011E+00	1.0016E+00	1.0025E+00	0.10
9.9885E-01	9.9995E-01	1.0011E+00	1.0023E+00	1.0036E+00	1.0055E+00	0.15
9.9762E-01	9.9961E-01	1.0017E+00	1.0039E+00	1.0061E+00	1.0097E+00	0.20
9.9562E-01	9.9875E-01	1.0021E+00	1.0056E+00	1.0091E+00	1.0149E+00	0.25
9.9247E-01	9.9702E-01	1.0019E+00	1.0070E+00	1.0123E+00	1.0208E+00	0.30
9.8770E-01	9.9396E-01	1.0007E+00	1.0078E+00	1.0153E+00	1.0274E+00	0.35
9.8069E-01	9.8892E-01	9.9786E-01	1.0074E+00	1.0175E+00	1.0341E+00	0.40
9.7065E-01	9.8111E-01	9.9260E-01	1.0050E+00	1.0182E+00	1.0403E+00	0.45
9.5659E-01	9.6948E-01	9.8383E-01	9.9956E-01	1.0165E+00	1.0454E+00	0.50
9.3725E-01	9.5270E-01	9.7016E-01	9.8964E-01	1.0110E+00	1.0481E+00	0.55
9.1112E-01	9.2909E-01	9.4981E-01	9.7341E-01	9.9983E-01	1.0470E+00	0.60
8.7630E-01	8.9652E-01	9.2046E-01	9.4846E-01	9.8064E-01	1.0399E+00	0.65
8.3048E-01	8.5236E-01	8.7917E-01	9.1165E-01	9.5022E-01	1.0240E+00	0.70
7.7088E-01	7.9330E-01	8.2221E-01	8.5893E-01	9.0443E-01	9.9554E-01	0.75
6.9412E-01	7.1530E-01	7.4490E-01	7.8515E-01	8.3788E-01	9.4950E-01	0.80
5.9617E-01	6.1337E-01	6.4137E-01	6.8376E-01	7.4368E-01	8.7942E-01	0.85
4.7221E-01	4.8142E-01	5.0432E-01	5.4649E-01	6.1304E-01	7.7698E-01	0.90
3.1652E-01	3.1206E-01	3.2477E-01	3.6305E-01	4.3490E-01	6.3151E-01	0.95
1.2235E-01	9.6354E-02	9.1663E-02	1.2064E-01	1.9540E-01	4.2958E-01	1.00

$H_z(z/a_1, 0)/H_0$

$\beta_g = 0.50$	$\beta_g = 0.45$	$\beta_g = 0.40$	$\beta_g = 0.35$	$\beta_g = 0.30$	$\beta_g = 0.22$	z/a_1
1.0002E+00	9.9996E-01	9.9970E-01	9.9944E-01	9.9917E-01	9.9875E-01	0.05
1.0007E+00	9.9974E-01	9.9873E-01	9.9768E-01	9.9663E-01	9.9496E-01	0.10
1.0013E+00	9.9912E-01	9.9686E-01	9.9455E-01	9.9221E-01	9.8855E-01	0.15
1.0015E+00	9.9770E-01	9.9377E-01	9.8974E-01	9.8569E-01	9.7937E-01	0.20
1.0008E+00	9.9503E-01	9.8901E-01	9.8289E-01	9.7678E-01	9.6728E-01	0.25
9.9873E-01	9.9054E-01	9.8213E-01	9.7362E-01	9.6517E-01	9.5213E-01	0.30
9.9453E-01	9.8370E-01	9.7625E-01	9.6156E-01	9.5060E-01	9.3383E-01	0.35
9.8764E-01	9.7399E-01	9.6016E-01	9.4637E-01	9.3284E-01	9.1232E-01	0.40
9.7760E-01	9.6102E-01	9.4435E-01	9.2784E-01	9.1177E-01	8.8760E-01	0.45
9.6409E-01	9.4456E-01	9.2505E-01	9.0585E-01	8.8729E-01	8.5968E-01	0.50
9.4707E-01	9.2458E-01	9.0223E-01	8.8035E-01	8.5934E-01	8.2849E-01	0.55
9.2682E-01	9.0132E-01	8.7601E-01	8.5133E-01	8.2777E-01	7.9376E-01	0.60
9.0403E-01	8.7528E-01	8.4663E-01	8.1867E-01	7.9216E-01	7.5477E-01	0.65
8.7989E-01	8.4721E-01	8.1428E-01	7.8199E-01	7.5156E-01	7.1005E-01	0.70
8.5613E-01	8.1811E-01	7.7903E-01	7.4036E-01	7.0414E-01	6.5693E-01	0.75
8.3508E-01	7.8909E-01	7.4056E-01	6.9193E-01	6.4669E-01	5.9097E-01	0.80
8.1971E-01	7.6130E-01	6.9783E-01	6.3342E-01	5.7398E-01	5.0524E-01	0.85
8.1365E-01	7.3568E-01	6.4869E-01	5.5953E-01	4.7794E-01	3.8934E-01	0.90
8.2120E-01	7.1274E-01	5.8933E-01	4.6207E-01	3.4665E-01	2.2831E-01	0.95
8.4728E-01	6.9223E-01	5.1361E-01	3.2904E-01	1.6311E-01	1.1938E-03	1.00

Table 9: Error coefficients $F_0E_n(\alpha, \beta) - F_gE_n(\alpha, \beta_g)$ for n = 0(zeroth), 2(second), 4(fourth), 6(sixth) and 8(eighth) for a coaxially displaced coil pair

$\alpha = 1.01, \beta = 0.5, \beta_g = 0.35$

r/a_1	zeroth	second	fourth	sixth	eighth
0.05	1.4646E-03	-1.1488E-06	-7.3922E-09	3.1827E-11	-6.2614E-14
0.10	1.4646E-03	-4.5953E-06	-1.1828E-07	2.0369E-09	-1.6029E-11
0.15	1.4646E-03	-1.0339E-05	-5.9877E-07	2.3202E-08	-4.1081E-10
0.20	1.4646E-03	-1.8381E-05	-1.8924E-06	1.3036E-07	-4.1035E-09
0.25	1.4646E-03	-2.8721E-05	-4.6202E-06	4.9730E-07	-2.4459E-08
0.30	1.4646E-03	-4.1358E-05	-9.5803E-06	1.4849E-06	-1.0517E-07
0.35	1.4646E-03	-5.6292E-05	-1.7749E-05	3.7444E-06	-3.6096E-07
0.40	1.4646E-03	-7.3525E-05	-3.0279E-05	8.3433E-06	-1.0505E-06
0.45	1.4646E-03	-9.3055E-05	-4.8501E-05	1.6914E-05	-2.6953E-06
0.50	1.4646E-03	-1.1488E-04	-7.3922E-05	3.1827E-05	-6.2614E-06
0.55	1.4646E-03	-1.3901E-04	-1.0823E-04	5.6384E-05	-1.3422E-05
0.60	1.4646E-03	-1.6543E-04	-1.5329E-04	9.5305E-05	-2.6923E-05
0.65	1.4646E-03	-1.9415E-04	-2.1113E-04	1.5362E-04	-5.1076E-05
0.70	1.4646E-03	-2.2517E-04	-2.8398E-04	2.3964E-04	-9.2405E-05
0.75	1.4646E-03	-2.5848E-04	-3.7423E-04	3.6253E-04	-1.6047E-04
0.80	1.4646E-03	-2.9410E-04	-4.8446E-04	5.3397E-04	-2.6893E-04
0.85	1.4646E-03	-3.3201E-04	-6.1741E-04	7.6823E-04	-4.3678E-04
0.90	1.4646E-03	-3.7222E-04	-7.7601E-04	1.0825E-03	-6.9001E-04
0.95	1.4646E-03	-4.1472E-04	-9.6337E-04	1.4973E-03	-1.0634E-03
1.00	1.4646E-03	-4.5953E-04	-1.1828E-03	2.0369E-03	-1.6029E-03

$\alpha = 1.01, \beta = 0.55, \beta_g = 0.40$

r/a_1	zeroth	second	fourth	sixth	eighth
0.05	1.3858E-03	-4.0654E-07	-8.7867E-09	2.8198E-11	-3.5557E-14
0.10	1.3858E-03	-1.6258E-06	-1.4059E-07	1.8047E-09	-9.1026E-12
0.15	1.3858E-03	-3.6580E-06	-7.1172E-07	2.0556E-08	-2.3329E-10
0.20	1.3858E-03	-6.5031E-06	-2.2494E-06	1.1550E-07	-2.3303E-09
0.25	1.3858E-03	-1.0161E-05	-5.4917E-06	4.4059E-07	-1.3889E-08
0.30	1.3858E-03	-1.4632E-05	-1.1388E-05	1.3156E-06	-5.9722E-08
0.35	1.3858E-03	-1.9916E-05	-2.1097E-05	3.3175E-06	-2.0498E-07
0.40	1.3858E-03	-2.6013E-05	-3.5990E-05	7.3919E-06	-5.9665E-07
0.45	1.3858E-03	-3.2922E-05	-5.7650E-05	1.4986E-05	-1.5306E-06
0.50	1.3858E-03	-4.0645E-05	-8.7867E-05	2.8198E-05	-3.5557E-06
0.55	1.3858E-03	-4.9180E-05	-1.2865E-04	4.9954E-05	-7.6219E-06
0.60	1.3858E-03	-5.8528E-05	-1.8220E-04	8.4199E-05	-1.5289E-05
0.65	1.3858E-03	-6.8689E-05	-2.5096E-04	1.3611E-04	-2.9005E-05
0.70	1.3858E-03	-7.9663E-05	-3.3755E-04	2.1232E-04	-5.2475E-05
0.75	1.3858E-03	-9.1450E-05	-4.4483E-04	3.2119E-04	-9.1128E-05
0.80	1.3858E-03	-1.0405E-04	-5.7585E-04	4.7308E-04	-1.5272E-04
0.85	1.3858E-03	-1.1746E-04	-7.3388E-04	6.8063E-04	-2.4804E-04
0.90	1.3858E-03	-1.3169E-04	-9.2240E-04	9.5908E-04	-3.9184E-04
0.95	1.3858E-03	-1.4673E-04	-1.1451E-03	1.3266E-03	-6.0388E-04
1.00	1.3858E-03	-1.6258E-04	-1.4059E-03	1.8047E-03	-9.1026E-04

3.7 *Axial Field Flux in the Midplane Between a Pair of Coils*

From Figures 24 and 25, it is clear that if the axial field $H_z(r/a_1, \pi/2)$ was integrated, then there would be a partial cancellation of fields greater than H_0 with those less than H_0. Ultimately, in the course of calibrating an induction coil placed between a pair of coils, the required experimental quantity is the flux $\int B\, dA$. Referring to Figure 24 for example, one could choose smaller values of β_g ($\beta_g < 0.3$) and maintain an averaged uniformity over a larger area by increasing r/a_1. However, this leads to undesirable large positive and negative variations in $H_z(r/a_1, \pi/2)/H_0$ from unity. Furthermore, beyond a certain r/a_1 value, the field deviation drops off very quickly and good uniformity cannot be achieved.

Because of cylindrical symmetry, it is possible to obtain a simple expression for the flux of the axial field in the mid-plane of the coil gap, $\Phi = \mu_0 2\pi \int H_z(\xi, \pi/2)\xi\, d\xi$. Here the zonal harmonic expansion form is convenient because the field geometry factors, Table 2, are independent of ξ. The flux Φ normalized to that of a uniform field (Φ_0) obtains from equations 33 and 38,

$$\frac{\Phi}{\Phi_0} = \frac{1}{F_0 - F_g}\left([F_0 - F_g] - \frac{\xi^2}{4}[F_0 E_2(\alpha,\beta) - F_g E_2(\alpha_g,\beta_g)] \right.$$
$$+ \frac{3\xi^4}{24}[F_0 E_4(\alpha,\beta) - F_g E_4(\alpha_g,\beta_g)] - \frac{5\xi^6}{64}[F_0 E_6(\alpha,\beta) - F_g E_6(\alpha_g,\beta_g)] \quad (40)$$
$$\left. + \frac{35\xi^8}{640}[F_0 E_8(\alpha,\beta) - F_g E_8(\alpha_g,\beta_g)] - \ldots \right).$$

For $\alpha = 1.01$, $\beta = 0.5$ and $\beta_g = 0.35$ (Fig. 24), $H_z(0.65, \pi/2)$ differs by 3% from H_0, but the flux within the central mid-plane region bounded by a circle of radius $0.65\, a_1$ differs by only 0.5% from the flux of a homogeneous field. Typical values of $\{(r/a_1), \Phi/\Phi_0\}$ evaluated for the above coil geometry from eqn. 40 are as follows: (0.3), 1.0062; (0.4), 1.0095; (0.5), 1.0114; (0.5726)[1], 1.0103; (0.6), 1.0091; (0.65), 1.0050 and (0.7), 0.9979. For $\alpha = 1.01$, $\beta = 0.55$ and $\beta_g = 0.4$, coil geometry (Fig. 25), typical values of $\{(r/a_1), \Phi/\Phi_0\}$ are: (0.2), 1.0010; (0.3), 1.0015; (0.4), 1.0010; (0.45), 0.9998; (0.5), 0.9977 and (0.6), 0.9887.

[1] $(H_z(r/a_1, \pi/2)/H_0) = 1.00$

4. Helmholtz Coil Apparatus

4.1 Introduction

Based on the computations given in section 3, a Helmholtz coil pair was constructed to provide good field uniformity over radial distances of approximately one metre. Since the lengths of the coils which require calibrating will be short, the field homogeneity $H_z(z/a_1, 0)/H_0$ above and below the central plane of the coil pair is not critical. Furthermore, in order to calibrate smaller coils with radii significantly less than one metre, it was decided to have a second coil gap setting such that the field homogeneity could be improved.

4.1.1 Physical Description of Coil Pair

A Helmholtz coil pair was constructed in order to achieve the field homogeneity predicted in Figures 24 and 25, specifically $\alpha = 1.01$, $\beta = 0.50$, $\beta_g = 0.35$ and $\alpha = 1.01$, $\beta = 0.55$, $\beta_g = 0.40$ where $a_1 = 99$ cm and consequently $a_2 = 99.99 \approx 100$ cm. This leads to an overall coil length (including gap) and gap spacing of 99 cm, 69.3 cm and 108.9 cm, 79.2 cm respectively for the above mentioned β, β_g values. The cross-section in each coil is a rectangle 1 cm by 14.85 cm.

The 2 m diameter coil pair needed to be placed in a stable frame to ensure the correct coil spacing while allowing easy access for coils which require calibrating. The framework consisted of four stout vertical wooden posts which supported two square wooden platforms. These in turn secured the coils, maintained the correct coil gap and held the vertical posts in a rigid framework. The entire structure was made from timber, glue and nylon bolts. Within the coil gap, two horizontal stout timber beams were cross-braced diagonally to the vertical posts. This structure which was vertically adjustable formed the support for the coil which was being calibrated.

The two square platforms which support the coils contain wooden dowel pegs at 20° spacings in the form of a circle. The pegs have two functions; firstly to secure the coils in the correct position such that the coil pair is concentrically aligned along the vertical axis. Secondly, the two square platforms when bolted together make up the demountable former upon which both coils were wound. Here the pegs hold the cheeks apart at the correct spacing and also interlock at 10° spacings to provide the pseudo circular support for a plastic strip which forms the mandrel. This technique enables both coils to be wound on the same coil former thus helping to preserve the same geometry.

A horizontal coil pair configuration, rather than a vertical one, enables a more even weight distribution of the coils[2] and also allows the coil which requires calibrating to be more easily aligned. In order to minimize weight, aluminium wire was chosen instead of copper because its density is less than one third of

[2] The coils would not be able to support their own weight in a vertical configuration and would thus require further structural support.

copper. An alternative would be to use plastic insulated wire. This has the advantage of requiring fewer turns of wire for the same α, β parameters, the only difference being the larger space packing factor associated with the plastic coated wire compared to enamelled wire. It is worth noting that for plastic insulated wire the diameter tolerances of the conducting filaments can be as low as 7% according to Cable Makers of Australia. This error might be expected to lead to an overall error in H_z because of the dependence of j_c and λ on the conductor cross sectional area. The homogeneity is unaffected. However $j_c\lambda$ determines the overall current density $NI/[2b(a_2 - a_1)]$, and the error reduces to that of $2b(a_2 - a_1)$. Furthermore, the small deviation from uniform current density distribution caused by the deviation in wire diameter would be small over the large dimensions of the coils.

The coils were wound with 2.00 mm diameter grade 2 polyester imide enamelled aluminium wire having the following properties: $\rho_{Al} = 2.824 \times 10^{-8}$ Ω m at 20°C, $d_{Al} = 2.7 \times 10^3$ kg m^{-3}, R ≈ 9×10^{-3} Ω m^{-1}, 4.7 turns per cm and 20 turns/cm^2. This implies $\lambda = 0.63$, $M_{Al} = 16.8$ kg, R ≈ 17.80 Ω and N ≈ 300 turns. These figures refer to each individual coil.[3]

4.1.2 *Coil Inductance and Mutual Inductance*

In order to minimize the inter-winding capacitance, inductance and coil winding effort, thick wire was used instead of thin wire. The inductance (H) for an individual coil was computed from Wheelers' formula for short coils [8]

$$L = 2.916 \times 10^{-6} N^2 \bar{r} \log_{10}\left[\frac{4.9\bar{r}}{(a_2 - a_1 + 2b)}\right] \qquad (41)$$

which gives 0.48 H for the above coils (N = 333) and compares favourably with the measured inductance of 0.47 H. In eqn. 41, r is the mean coil radius, $(a_2 + a_1)/2$. The mutual inductance M was computed from expressions with tabulated coefficients representative of coil geometry [9] and gave $M = 0.0696$ H for coils of rectangular cross-sections. (The same result obtains with the two coils each represented by a single circular filament multiplied by the square of the number of turns.) By measuring the inductance of the coil pair, both series aiding and series opposing, the mutual inductance was determined to be 0.068 ± 0.016 H.

[3] The two coils were individually wound with five layers and a total number of turns $N = 333$.

4.2 *Theoretical Fields*

4.2.1 *Field at Centre of a Non-zero Cross-section Coil*

As an approximation, a coil can be replaced by a single filamentary loop where the loop radius a is $(a_2 + a_1)/2$. From eqn. 2 at $N = 333$, $B_z(0, 0) = [2.103 \times 10^{-4} I]$ T. For a coil of non-zero cross-section with the above parameters, eqn. 7 leads to $B_z(0, 0) = [2.118 \times 10^{-4} I]$ T where $\alpha = (100/99) = 1.0101$. The single filamentary loop coil underestimates the central field by less than 1%.

4.2.2 *Field at Centre of Coaxially Displaced Coils*

From eqn. 33, the field at the centre of the gap for a pair of coils is given by $B_z(0, 0) = [3.284 \times 10^{-4} I]$ T for $\alpha = 1.01$, $\beta = 0.50$, $\beta_g = 0.35$ and $B_z(0, 0) = [3.107 \times 10^{-4} I]$ T for $\alpha = 1.01$, $\beta = 0.55$, $\beta_g = 0.40$. The central field of the Helmholtz coil is 55% or 47% higher than the single coil depending on the gap.

4.3 *Determination of the Calibrating Field*

4.3.1 *Search Coil*

The field at the centre of the coil pair can be predicted from the expressions for $B_z(0, 0)$ in section 4.2.2 from the current in the coils which can be monitored from the voltage across a 1 Ω resistor in series with the coils. The resonant frequency of the coil pair and the individual coils was measured at about 2.1 kHz. Thus the predicted field would not be expected to be accurate above frequencies where the inter-winding capacitance shunts the current across the coil. In this case the voltage drop across the 1 Ω sense resistor does not give a true indication of the current in the windings and hence of the magnetic field. Furthermore, introducing a coil at the centre of the gap can further load the Helmholtz coils at and above the resonant frequency of the centre coil. Even if the centre coil is open circuit, it acts as a shorted turn at the coil centre above resonance.

A convenient method of determining the calibration field is to use a single layer search coil wound on a non metallic tube. The voltage induced by a sinusoidal magnetic field at frequency f, orthogonal to the plane of the search coil windings is

$$V = 2N\pi^2 r^2 f B \tag{42}$$

where r is the radius of the winding in metres, B is in tesla and V is in volts. One hundred turns of 38 S.W.G. enamelled copper wire was wound on a PVC tube having an outside diameter of 155.5 mm. The search coil calibration

factor is 11.93 V T^{-1} Hz^{-1} or equivalently

$$B = 8.381 \times 10^{-2} \frac{V}{f}. \tag{43}$$

The resonant frequency, 7.5 MHz, of the search coil lies well above the Helmholtz coil resonance. (A less sensitive search coil wound with a hundred turns (38 S.W.G.) on 25.4 mm diameter rod, having a calibration factor of 0.3184 V T^{-1} Hz^{-1} was also used.)

4.3.2 Comparison of Search Coil Measurements and Theoretical Expressions

In the following discussion, $B_c^{\#2}$ refers to the field determined from measurements taken with the more sensitive search coil (eqn. 43) and $B_c^{\#1}$ refers to measurements taken with the smaller less sensitive search coil. In addition, $B_{1\Omega}$ refers to the field at the coil pair centre obtained from the theoretical expression, $B_z(0, 0) = 3.284 \times 10^{-4} I$ T, by measuring the voltage drop across the one ohm resistor in series with the coil pair windings. All voltages were measured with a spectrum analyser.[4]

Below about 500 Hz, determinations of the central field, with search coils and from the theoretical expressions gave agreement within 4% or better. The discrepancy at higher frequencies is illustrated in Figure 26 which plots $B_c^{\#2}/B_{1\Omega}$ as a function of frequency. Similar results obtain for $B_c^{\#1}/B_{1\Omega}$. Clearly, above 500 to 600 Hz, the determination of the central field from the measurement of the Helmholtz coil current is inaccurate. This frequency range is further reduced if the central coil which requires calibration has a resonance frequency below the Helmholtz coil pair resonance frequency.

4.3.3 Comparisons with Fluxgate Magnetometers

The field from the Helmholtz coil pair was also measured with a Domain magnetic underwater sensor (MUWS1 triaxial fluxgate system) and a less sensitive fluxgate probe (Institut Dr Forster Magnotoscop 1.068). The field measured by these two sensors are designed B_z and B_F respectively. The only significant restriction with these two instruments is that they are limited to low frequency operation, especially the MUWS1. Measurements were taken at 1 Hz and 0.5 Hz over a range of coil currents with care being taken not to saturate the MUWS1 sensor. The estimated errors are $B_c^{\#1}/B_{1\Omega}$: ± 3%, $B_F/B_{1\Omega}$: ± 3%, and $B_z/B_{1\Omega}$: ± 2%. Good agreement to within experimental error was found between $B_{1\Omega}$ and B_z and between $B_{1\Omega}$ and B_F. Reasonably good agreement was also found for $B_c^{\#2}/B_{1\Omega}$ (1.043 ± 0.020).

[4] In this way one instrument allowed measurement of voltages over the extremely low frequency range and furthermore, the waveform could be monitored to allow for distortion or non-linearities.

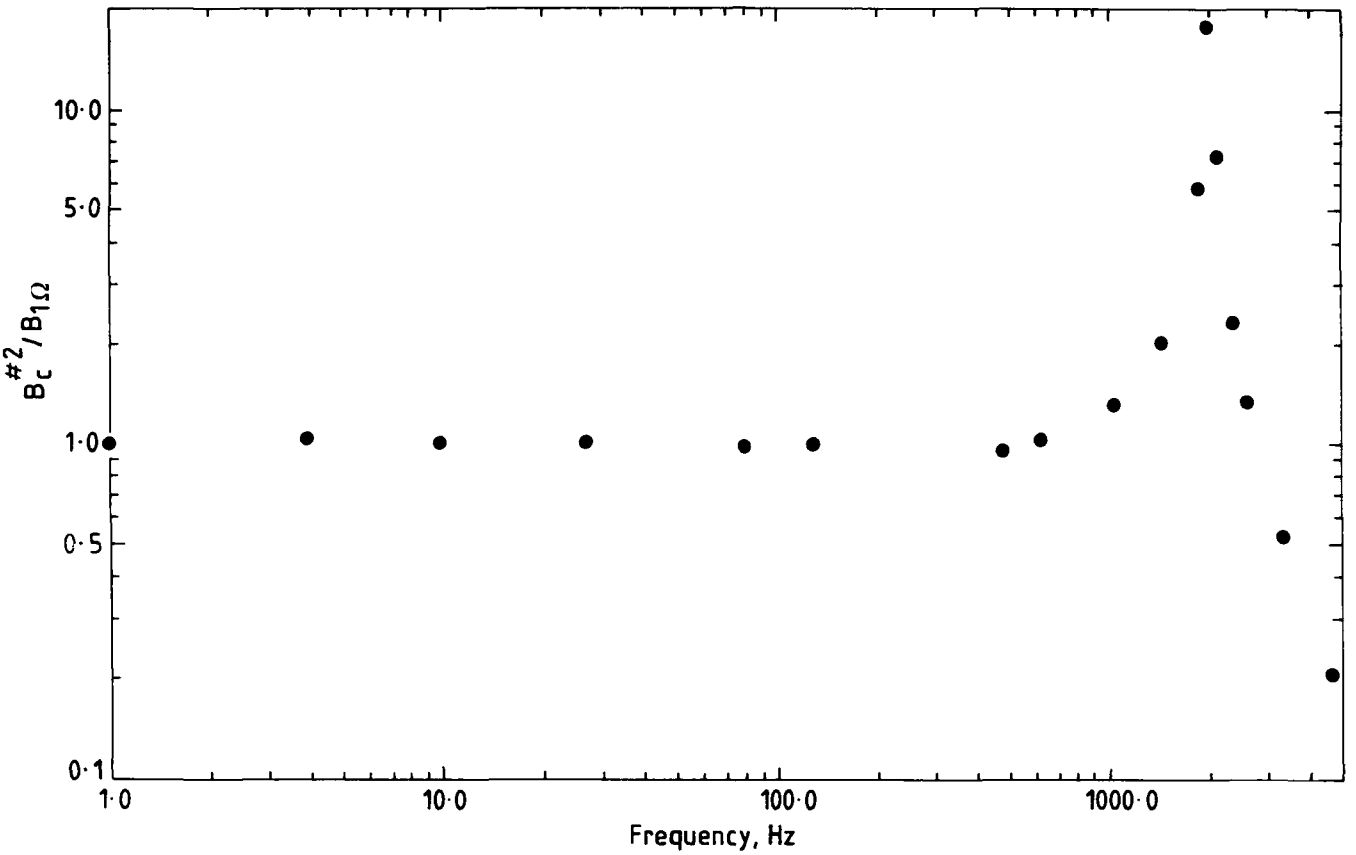

Figure 26: Ratio of magnetic field measured with search coil ($B_c^{\#2}$) to that measured from current in Helmholtz coil ($B_{1\Omega}$) as a function of frequency. (At high frequencies, $B_{1\Omega}$ is not derived from the current in the coil).

The above measurements were restricted to $f \leq 1.0$ Hz. At higher frequencies up to 100 Hz, the search coil field measurements were checked with a known calibrated field generated by the vertical component of the three axis cube arrangement of the magnetic facility at the Shark Point degaussing range, Sydney.[5] A series of magnetic field measurements with both search coils reveal an agreement generally within ± 2% of the computed field at the centre of the cube.

[5] Here, agreement to within 1% was found with the MUWS1 at 0.5 Hz.

4.4 *Field Homogeneity*

The field homogeneity of the coil pair is readily determined by taking field measurements using a search coil at known distances along one of the arms of the cross-beams, see 4.1.1. The search coil windings are located in the central plane between the Helmholtz coil pair. Measurements were also taken for displacements above the centre of the coil pair. Thus the theoretical curves of $H_z(r/a_1, \pi/2)/H_0$ and $H_z(z/a_1, 0)/H_0$ in Figure 24 can be verified experimentally. The results of the field uniformity tests are given in Table 10. They show excellent agreement with the theoretical curves.

Table 10: Magnetic field homogeneity assuming $\alpha = 1.01$, $\beta = 0.5$, $\beta_g = 0.35$, *Figure 24*

$H_z(\xi, \pi/2)/H_0$		ξ
Experimental	Theoretical (Table 3.2)	
1.0	1.0	0.0
1.0	1.002	0.1
1.0	1.006	0.2
1.012	1.011	0.3
1.012	1.015	0.4
1.012	1.012	0.5
0.977	0.992	0.6
0.923	0.936	0.7
0.813	0.812	0.8
0.603	0.569	0.9
$H_z(\gamma, 0)/H_0$		γ
Experimental	Theoretical (Table 3.2)	
1.0	1.0	0.0
0.994	0.997	0.1
0.977	0.986	0.2
0.966	0.966	0.3

5. *Conclusion*

The design for air-core uniform current density coils is discussed in terms of coil geometry. This enables the field at the centre of the coil (H_0) to be computed or determined graphically from Figures 3 and 4.

The magnetic field within the region of the coil centre is evaluated using Garrett's [3] zonal hormonic expansion technique. This enables the radial and

axial fields to be expressed as a sum of terms involving geometry factors and normalized distances. The direct dependence of the field expressions on H_0 allows the field homogeneity to be conveniently expressed in terms of geometry factors alone. Suitable convergence of the series expansion must be achieved. Table 3 gives the individual contributions of the second-, fourth-, sixth- and eighth-order terms over a wide range of coil geometries. Several important examples are given in Figures 6 to 8.

Hart's [2] method for computing the radial and axial fields is also discussed. This involves a direct evaluation of the field by numerical integration of a volume element within the coil. A comparison of this method is made with the zonal harmonic expansion approach. The former technique is a useful computational method for an individual coil geometry but, unlike the expansion method, is not suited for modelling studies.

The superposition principle and symmetry arguments are next employed to compute the axial fields along the axis of two coaxially displaced coils. A comparison of the field homogeneity generated by this system with that of a single coil reveals the improvement offered by a two-coil system.

The effectiveness of the zonal harmonic expansion method becomes more apparent when it is applied to the multiple coil system to provide expressions for the fields and their homogeneity within the central region of the gap formed by the pair of coils. The correct gap width for maximum homogeneity or for perfectly compensated coils can be obtained either graphically (Figs 19 to 22) or numerically. The graphical approach gives a good approximate result and clearly shows the correct gap setting as a function of coil geometry. A particular result that emerges from Figures 19 and 21 is that by choosing a value of β such that $F\,E_2(\alpha, \beta)$ is a minimum, then for small α, the correct Helmholtz coil gap equals the internal radius of short coils, $\beta_g \approx \beta$. The deviations associated with this rule of thumb for larger values of α can also be gauged from Figures 19 to 22.

The numerical solution of the correct gap setting for fourth-order compensated coils allows the contributions of the remaining higher order terms to be automatically determined. This allows the computation and tabulation of error limits for different coil geometries (Table 6).

Equations 32 and 33 allow modelling of the field homogeneity for a wide range of gap settings. Fourth-order compensation is included by substituting the required β_g value, see Figures 19 to 22 and section 3.4. The resultant field homogeneities $H_z(r/a_1, \pi/2)/H_0$ are plotted so as to examine the trade-off obtained by achieving a larger area of field uniformity at the expense of degrading the degree of field uniformity. Depending upon the application, this can be advantageous since the total flux of the axial field in the midplane can approach the value that would exist for a perfectly uniform field because of the partial cancellation of the positive and negative areas enclosed by the $H_z(r/a_1, \pi/2)/H_0$ versus r/a_1 curves. This advantage does not apply to the monotonically decreasing function $H_z(z/a_1, 0)/H_0$.

In section 4, a physical description and construction details are given for a coil pair based on the theoretical expressions developed in section 3. The field predictions were checked with the aid of two search coils and two fluxgate magnetometers. Agreement between theory and experiment lies within 4%. Furthermore, the field homogeneity was found to be in excellent agreement with theoretical expectations.

6. *Acknowledgement*

I wish to thank Pat Vlaming for her skilful and dedicated preparation of the artwork.

7. *References*

1. Montgomery, D.B. (1969).
Solenoid magnet design - the magnetic and mechanical aspects of resistive and superconducting systems. New York: Wiley-Interscience.

2. Hart, P.J. (1967).
Universal tables for magnetic fields of filamentary and distributed circular currents. New York: Elsevier Publishing Company.

3. Garrett, M.W. (1951).
Axially symmetric systems for generating and measuring magnetic fields, Part I. *Journal of Applied Physics,* Vol. 22, p. 1091.

4. Garrett, M.W. (1963).
Calculation of fields, forces, and mutual inductances of current systems by elliptic integrals. *Journal of Applied Physics,* Vol. 34, p. 2567.

5. Montgomery, D.B. and Terrell, J. (1961).
Some useful information for the design of air-core solenoids (Report AFOSR-1525). Massachusetts: National Magnet Laboratory, Massachusetts Institute of Technology.

6. Girard, B. and Sauzade, M. (1964).
Calcul des solenoides compenses du 6eme ordre, a volume de bobinage minimum. *Nuclear Instruments and Methods,* Vol. 25, p. 269.

7. Dorn, W.S. and McCracken, D.D. (1972).
Numerical methods with Fortran IV case studies. New York: Wiley International.

8. Langford-Smith, F. (Ed.) (1957).
Radiotron designer's handbook, Fourth Edition. Sydney: Wireless Press (Amalgamated Wireless Valve Co Pty Ltd).

9. Grover, F.W. (1946).
Inductance calculations. New York: D. Van Nostrand Co.

Appendix A

Numerical Computations

Fortran source code (HELMHZ.for) was developed for evaluating the axial field deviation from the central field for a Helmholtz coil. The percentage deviation from the central field is read in as the variable **ERROR**. The variable **DELTA** determines the tolerance in the Newton-Raphson solution for determining β_g. Sample computations are shown in Table 6.

Fortran source code (HSPLIT.for) was also written to compute the deviation of the axial magnetic field from the central field at points located along the axis, $H_z(z/a_1, 0)/H_0$ and radially away from the gap centre, $H_z(r/a_1, \pi/2)/H_0$. H_0 refers to the axial field at the centre of the gap. Computations are carried out over a range of specified β_g values for a given α, β value; α, β and β_g are defined in Figure A.1. (Unlike Figure 14, 2β is equivalent to the *overall* coil length including the gap, whereas previously in Figure 14, 2β referred to the length of each individual coil).

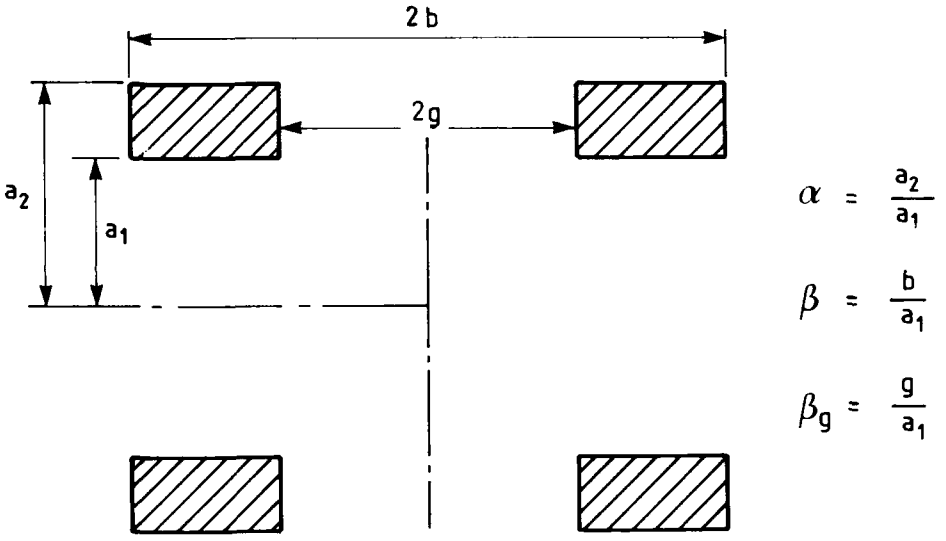

Figure A.1: Coaxial coil pair.

The following variables are required from a data file,

AC, BC	:	the α, β values
GMIN	:	the initial value of ρ/a_1 (z/a_1 or r/a_1)
NGAMMA	:	the number of increments in ρ/a_1
DELG	:	the ρ/a_1 increment
NBGAP	:	the number of β_g values
BETA(I)	:	the β_g values

A subroutine COEFS computes the required error coefficients $F(\alpha, \beta)$, $FE_2(\alpha, \beta)$ ....$FE_8(\alpha, \beta)$ in double precision.

These programmes may be requested from the author if desired.

DOCUMENT CONTROL DATA SHEET

REPORT NO.	AR NO.	REPORT SECURITY CLASSIFICATION
MRL-TR-91-8	AR-006-355	Unclassified

TITLE

Magnetic field distribution within uniform current density coils of non-zero cross-section and the design of Helmholtz coils

AUTHOR(S)
Julian Vrbancich

CORPORATE AUTHOR
Materials Research Laboratory
PO Box 50
Ascot Vale Victoria 3032

REPORT DATE	TASK NO.	SPONSOR
April, 1991	DST 86/149	DSTO

FILE NO.	REFERENCES	PAGES
G6/4/8-3537	9	61

CLASSIFICATION/LIMITATION REVIEW DATE

CLASSIFICATION/RELEASE AUTHORITY
Chief, Underwater Systems Division

SECONDARY DISTRIBUTION

Approved for public release

ANNOUNCEMENT

Announcement of this report is unlimited

KEYWORDS

Uniform magnetic fields
Electromagnet
Helmholtz coils
Magnet coils

ABSTRACT

A uniform magnetic field is required to calibrate magnetic induction sensor coils. Two types of coil designs are considered; a single finite length solenoid and a coaxially split coil pair (Helmholtz coil). The design must be able to reliably predict the magnitude of the calibration field and its homogeneity, both radially and axially, to within certain tolerances. The experimental results of a design based on the split coil pair are given. Furthermore, it is suggested that the quasi-uniform field in the mid-plane of a split coil pair can be usefully extended by narrowing the gap of the conventional Helmholtz coil pair spacing. In such cases, the flux in a circular region in the mid-plane can approach the value that would exist for a perfectly uniform field because of the partial cancellation between fields greater than and less than the central field. The deviation of the central field from that of an infinitely long solenoid is also discussed.